Placenta 29 (2008) 1003–1008

Contents lists available at ScienceDirect

Placenta

journal homepage: www.elsevier.com/locate/placenta

Long-term Forskolin Stimulation Induces AMPK Activation and Thereby Enhances Tight Junction Formation in Human Placental Trophoblast BeWo Cells

M. Egawa [a], H. Kamata [a], A. Kushiyama [b], H. Sakoda [c], M. Fujishiro [c], N. Horike [d], M. Yoneda [a], Y. Nakatsu [a], Guo Ying [a], Zhang Jun [a], Y. Tsuchiya [a], K. Takata [e], H. Kurihara [d], T. Asano [a,*]

[a] Department of Medical Chemistry, Division of Molecular Medical Science, Graduate School of Biomedical Science, Hiroshima University, 1-2-3 Kasumi, Minami-ku, Hiroshima City, Hiroshima 734-8551, Japan
[b] The Institute for Adult Diseases, Asahi Life Foundation, 1-6-1 Marunouchi, Tiyoda-ku, Tokyo 100-0005, Japan
[c] Department of Internal Medicine, Graduate School of Medicine and Faculty of Medicine, University of Tokyo, 7-3-1 Honga, Bunkyo-ku, Tokyo 113-0033, Japan
[d] Department of Physiological Chemistry and Metabolism, Graduate School of Medicine and Faculty of Medicine, University of Tokyo, 7-3-1 Hongo, Bunkyo-ku, Tokyo 113-0033, Japan
[e] Department of Cell Biology, Institute for Cellular and Molecular Regulation, Gunma University, 3-39-15 Showamachi, Maebashi, Gunma 371-8512, Japan

ARTICLE INFO

Article history:
Accepted 10 September 2008

Keywords:
BeWo cells
Forskolin
Tight junction
AMPK

ABSTRACT

BeWo cells, derived from human choriocarcinoma, have been known to respond to forskolin or cAMP analogues by differentiating into multinucleated cells- like syncytiotrophoblasts on the surfaces of chorionic villi of the human placenta. In this study, we demonstrated that long-term treatment with forskolin enhances the tight junction (TJ) formation in human placental BeWo cells. Interestingly, AMPK activation and phosphorylation of acetyl-CoA carboxylase (ACC), a molecule downstream from AMPK, were induced by long-term incubation (>12 h) with forskolin, despite not being induced by acute stimulation with forskolin. In addition, co-incubation with an AMPK inhibitor, compound C, as well as overexpression of an AMPK dominant negative mutant inhibited forskolin-induced TJ formation. Thus, although the molecular mechanism underlying AMPK activation via the forskolin stimulation is unclear, the TJ formation induced by forskolin is likely to be mediated by the AMPK pathway. Taking into consideration that TJs are present in the normal human placenta, this mechanism may be important for forming the placental barrier system between the fetal and maternal circulations.

1. Introduction

Epithelial cells are connected side-to-side by junctional complexes consisting of tight junctions (TJs), adherens junctions and desmosomes, and play fundamental roles in separating compositionally different compartments. This allows regulation of homeostasis and maintenance of physiological functions in multicellular organisms. Intercellular junction assembly is initiated by cadherin-mediated cell–cell contact, followed by formation of the adherens junctions and the assembly of desmosomes and TJs [1–4]. One of the notable features of epithelia is the capacity to create selective barriers. For example, intestinal epithelial cells prevent the ingress of luminal macromolecules and bacteria and protect against inflammation and infection [5], and brain endothelial cells form the blood–brain barrier which maintains intracerebral homeostasis and protects the brain from toxic substances [6].

The placenta is a haemochorial villous organ, and the chorionic villi, which are in direct contact with maternal blood, play an important role throughout pregnancy. Chorionic villi are covered with a syncytiotrophoblast layer comprised of epithelial cells, the site of nutrition supply to the growing fetus, gas exchange and the release of hormones into both maternal and fetal circulations [7]. In addition, syncytiotrophoblasts also play important roles such as providing a barrier against maternal pathogens and inhibiting paracellular diffusion of molecules. Indeed, previous studies have shown the presence of TJs in the syncytiotrophoblast layer [8].

Therefore, we focused on TJ formation in BeWo cells. The BeWo cell line used in this study was derived from human

* Corresponding author. Tel.: +81 82 257 5135; fax: +81 82 257 5136.
E-mail address: tasano@hiroshima-u.ac.jp (T. Asano).

0143-4004/$ – see front matter © 2008 Elsevier Ltd. All rights reserved.
doi:10.1016/j.placenta.2008.09.008

choriocarcinoma and differentiates into multinucleated cell-like syncytiotrophoblasts secreting human chorionic gonadotropin (hCG) in response to increased intracellular cAMP or forskolin stimulation [9–11]. Thus, BeWo cells have frequently been used to elucidate the molecular mechanisms underlying syncytialisation, a process by which the underlying cellular cytotrophoblasts are transformed into syncytiotrophoblasts.

However, we initially found that BeWo cells exhibited not only the above-mentioned differentiation into hCG-secreting syncytiotrophoblasts with cell fusion but also showed markedly enhanced formation of TJ strands, in response to forskolin stimulation. Based on a recent report, TJ assembly is regulated via AMPK activity [12,13]. However, to our knowledge, there are no reports showing forskolin stimulation to induce AMPK activation. Thus, we investigated whether AMPK activation is involved in the forskolin-induced TJ strand formation of BeWo cells, using the AMPK inhibitor compound C as well as various adenoviruses. Herein, we show that chronic stimulation with forskolin activates AMPK, in a fashion similar to that observed with 2-deoxy-D-glucose stimulation and that AMPK activation is necessary for forskolin-induced TJ formation by BeWo cells. This finding suggests that AMPK activity is a key regulator of TJ formation by syncytiotrophoblasts, and thereby ultimately affects placental barrier function.

2. Materials and methods

2.1. Cell culture and transfection

BeWo cells were maintained at 37 °C as monolayers in Ham's F-12K medium supplemented with 10% fetal bovine serum (FBS), 100 U/ml penicillin and 100 U/ml streptomycin in a humidified atmosphere of 5% CO_2 and 95% air. Cells were subcultured by treatment with 0.05% trypsin in Ca^{2+} and Mg^{2+} free phosphate buffered saline (PBS), seeded and grown to the 70% confluence stage. At the cell density of 70% confluence, agents such as 100 μM forskolin, 10 μM compound C, and 25 mM 2-deoxy-D-glucose were added to the medium and the cells were incubated for the indicated times. For transfection experiments, the cells were grown to 70% confluence and transfected with the indicated expression vectors in suspension with lipofectamine plus reagent (Invitrogen) according to the manufacturer's protocol.

2.2. Generation of recombinant adenoviruses

The cDNA encoding residues 1–312 of AMPKα1, containing a mutation that alters threonine 172 to an aspartic acid (T172D), was generated and its recombinant adenovirus produced, as described previously [14]. The cDNA encoding AMPKα1, containing a mutation that alters threonine residue 172 to alanine, was used to construct the dominant negative mutant (DNα1). Both constructs were designed to contain a c-myc tag at the NH_2 terminus. Adenoviruses expressing GFP were used as the control. The amplified adenoviruses were purified and concentrated using cesium chloride ultracentrifugation. The resultant viruses were then dialysed into PBS containing 10% glycerol.

2.3. Immunohistochemistry

Cells grown on cover glasses were rinsed with ice-cold PBS for 5 min, fixed for 15 min in 3% formaldehyde, and permeabilised for 5 min in PBS containing 0.1% Triton X-100. After washing, they were blocked in PBS containing 1% BSA for 1h. The primary rabbit anti-ZO-1 polyclonal antibody (1:500 dilution; Zymed, San Francisco, CA) was diluted in 1% BSA and incubated for 2 h at room temperature. The cover glasses were washed before incubation in secondary Cy3 goat anti-rabbit IgG (H + L) conjugate (1:1000 dilution; Zymed) with DAPI 0.5 μg/ml for 1 h at room temperature. All washings were performed using PBS containing 0.1% Tween 20 (PBS-T). The cover glasses were mounted in Fluoro Guard Antifade Reagent (Bio-Rad).

2.4. Triton X-100 extractability assay

Confluent monolayers of BeWo cells were subjected to the Triton X-100 extractability assay as previously described [15,16]. Monolayers were rinsed three times with ice-cold PBS and cells were then extracted for 15 min at 4 °C on a rotating platform after covering the cells with the buffer containing 0.5% Triton X-100, 100 mM NaCl, 10 mM Tris– HCl (pH 7.4), and 300 mM sucrose plus a protease inhibitor (1 mM phenylmethylsulfonyl fluoride). The extract fraction was completely aspirated and collected, and the residue fraction was separated by centrifugation at 15,000 × g for 20 min at 4 °C and then dissolved in Laemmli sample buffer. The samples were analysed by SDS-PAGE and Western immunoblotting.

2.5. Western immunoblotting

The cells were collected and boiled in Laemmli sample buffer containing 100 mM dithiothreitol. The proteins were separated by SDS-PAGE, and transferred to nitrocellulose membranes. To minimise non-specific binding, the membranes were blocked with 3% skimmed milk in PBS-T for 1 h. Then, the primary antibodies in PBS-T were added and the membranes were incubated overnight at 4 °C. The following antibodies were used: anti-ZO-1 antibody (1:2000 dilution; Zymed), anti- phospho-AMPKα (Thr172) antibody (1:2000 dilution; Cell Signaling Technology), anti-phos pho-acetyl-CoA carboxylase-α (ACC) (Ser79) antibody (1:2000 dilution; cell signaling technology), anti-AMPK antibody, and anti-CREB antibody. The membranes were washed in PBS-T before incubation in secondary horseradish peroxidase-labeled donkey anti-rabbit antibody (1:1000 dilution GE Healthcare, UK) for 1 h at room temperature. After washing, immunoreactive bands were visualised using an enzyme-linked chemiluminescence detection reagent (Pierce, Rockford, IL) and documented on autoradiographic films.

2.6. Luciferase assay

Cell extracts were prepared using cell culture lysis reagent (Promega, Madison, WI). Luciferase activity was measured according to the manufacturer's protocol (Promega) using a chemiluminescence detection system.

2.7. Quantitative reverse-transcription polymerase chain reaction (qPCR)

Expression of hCG mRNAs was measured by a reverse transcription polymerase chain reaction (RT-PCR) method. Total RNAs were extracted from BeWo cells with or without 100 μM of forskolin and/or 10 μM of compound C stimulation for 24 h, using TRIsure (Nippon Genetics, JP). One μg of total RNA was applied to obtain cDNA using a transcriptor cDNA first strand synthesis kit (Roche), and real-time PCR was then performed using FastStart SYBR Green Master (Roche) and the Light Cycler 2.0 system (Roche), according to the manufacturers' respective instructions. Primer sequences were as follows, human GAPDH forward: 5'-GCAGGGGGGAGCCAAAAGGGT-3', reverse: 5'-TGGGTGGCAGTGATGGCATGG-3', hCG forward: 5'-CCAAGGATGGAGATGTTCCAG-3', reverse: 5'-CTGCAGCACGCGGGTCATGGT-3'.

2.8. Cell fusion analysis

The rate of cell fusion (syncytialisation) was measured as described previously by flow cytometry [17]. Cloned BeWo cells expressing either a fusion protein of green fluorescent protein and human histone H2B (H2B-GFP) or a fusion protein of red fluorescent protein and the mitochondrial targeting sequence from subunit VIII of human cytochrome *c* oxidase (Mit-DsRed2) were mixed at 50% confluence. The medium was then changed to one containing 1 mM 5-aminoimidazole-4-carboxamide-1-β-D-ribofuranosyl 5'-monophosphate (AICAR), 10 μM compound C, and vehicle (DMSO). Two hours later, 100 μM forskolin or DMSO was added to the medium and the cells were incubated for 24 h, then harvested by trypsinisation, fixed and the numbers of single fluorescent (green or red) positive cells (i.e., non-fused or non-detectably fused cells) and double fluorescent (green and red) positive cells (i.e., detectably fused cells) were counted using a flow cytometer (BD FACSAria, Becton Dickinson, Franklin Lakes, NJ, USA). Ten thousand cells were analysed on each sample.

3. Results

3.1. Forskolin induces TJ assembly in BeWo cells

BeWo cells were treated with forskolin or DMSO (vehicle control) for 24 h, and ZO-1, one of the TJ component proteins [18,19], was visualised by immunofluorescence using anti-ZO-1 antibody. Forskolin treatment markedly enhanced the assembly of TJ strands, as shown by ZO-1 staining on the cell surface (right panel of Fig. 1A), while only weak ZO-1 staining was observed in control cells (left panel of Fig. 1A). To confirm this effect on TJ formation, we used the Triton X-100 extractability assay, a biochemical approach to analysing interactions between junctional proteins and the cytoskeleton. Prepared samples contain cytoskeleton-associated proteins, including TJ component proteins such as ZO-1. Thus, it is possible to evaluate the formation of TJ by measuring the ZO-1 content of Triton-insoluble pools. Fig. 1B shows that a 220-kd band corresponding to ZO-1 was markedly increased after 12 or 24 h incubation with forskolin. These results indicate that forskolin induces TJ formation in BeWo cells.

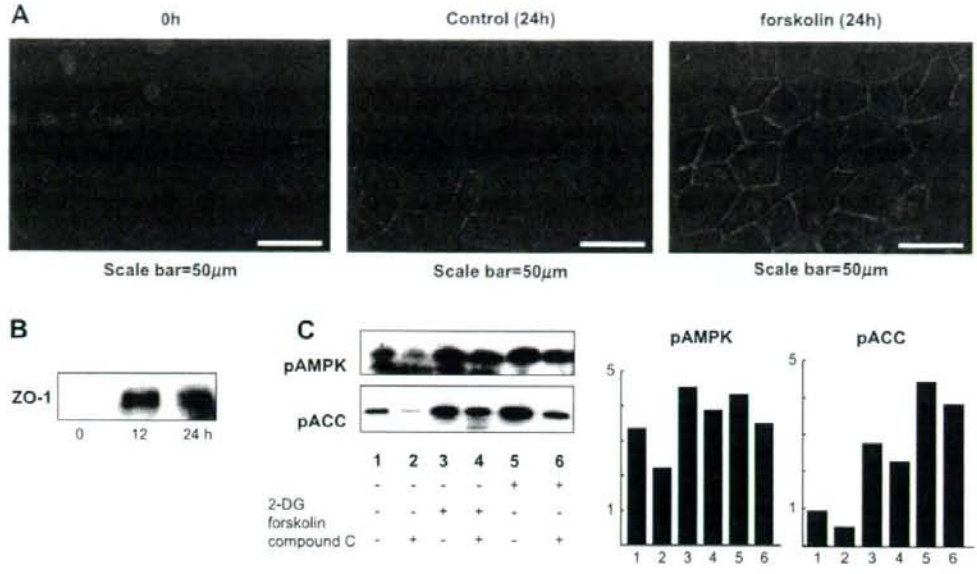

Fig. 1. Localisation and expression of ZO-1 in BeWo cells. A. Immunohistochemical localisation of ZO-1 in BeWo cells. Cells were cultured with 100 μM forskolin or vehicle for 24 h, and stained with a polyclonal antibody (1:500) against ZO-1 antibody (red), and counterstained with DAPI (blue fluorescence). ZO-1 was detected in the cell periphery. Forskolin treatment promoted assembly of TJ strands. B. BeWo cells treated with 100 μM forskolin were harvested at different time points, and ZO-1 protein expression was measured in the Triton X-100 extractability assay. ZO-1 protein expression was low or undetectable at 0 h, but had increased markedly after 12 h in culture and remained elevated at 24 h. C. BeWo cells were stimulated with 25 mM 2-deoxy-D-glucose, 100 μM forskolin or 10 μM of the selective AMPK inhibitor compound C, alone or in combination, for 12 h as indicated. Culture with vehicle (DMSO) served as the control (lane 1). Western blots detecting phosphorylated (Thr-172) AMPK antibody (1:2000) and phosphorylated (Ser79) Acetyl-CoA Carboxylase antibody (1:2000) were performed. The densitometric analysis of each protein is shown in the bar graph.

3.2. *Effect of forskolin on AMPK activation*

Subsequently, we examined whether forskolin affects AMPK activity. BeWo cells were stimulated with forskolin, 2-deoxy-D-glucose or the selective AMPK inhibitor compound C alone or in combination for 12 h, and phosphorylation of AMPK on the Thr172 residue, which is located within the activation loop of the catalytic subunit (upper panel of Fig. 1C), as well as phosphorylation of one of its cellular substrates, ACC (lower panel of Fig. 1C), were investigated [20]. 2-Deoxy-D-glucose, a sugar which cannot be metabolised, reportedly suppresses the glycolysis pathway, induces ATP depletion and activates AMPK [21]. As expected, 2-deoxy-D-glucose stimulated AMPK and ACC phosphorylation, and these effects were inhibited by compound C (lanes 5 and 6 of Fig. 1C). Interestingly, it was revealed that 12 h forskolin treatment also markedly stimulated AMPK and ACC phosphorylation (lane 3 of Fig. 1C). Similar to the observations made with 2-deoxy-D-glucose stimulation, co-incubation with compound C suppressed the phosphorylations of AMPK and ACC induced by forskolin (lane 4 of Fig. 1C).

3.3. *Activation of CRE-dependent transcription by forskolin*

Forskolin is known to increase intracellular cAMP. To examine this effect, we used BeWo cells transiently transfected with a CRE-luciferase reporter construct. CRE-Luc BeWo cell lines showed an approximately 3.7-fold increase in luciferase activity at 1 h after forskolin stimulation (Fig. 2A). Compound C partially inhibited the effect of forskolin, though we were not able to determine the underlying molecular mechanism. Forskolin also reportedly increases hCG, a placenta-derived hormone [22], mRNA levels via a rapid and transient induction of CRE-dependent transcription. Indeed, Fig. 2B shows hCG mRNA levels to increase approximately 12-fold with forskolin stimulation. Co-incubation with compound C significantly enhanced the forskolin-induced increase in hCG mRNA levels. Despite the mechanism underlying compound C-induced alterations in CRE activity and hCG mRNA expression, it is likely that compound C is neither a toxic agent nor a strong inhibitor of CRE-mediated gene expressions.

3.4. *Overexpression of constitutively active and dominant negative AMPKα1 in BeWo cells*

Adenovirus-mediated overexpressions of CAα1 (constitutively active AMPK) and D/Nα1 were detected by immunoblotting using the antibody against AMPK (upper panel of Fig. 3A). Since CAα1 is a truncated mutant of AMPKα1, it was detected as a band at a lower molecular weight than the endogenous subunit (lane 4) as reported previously [23]. A 63-kd band corresponding to D/Nα1 and a 31-kd band corresponding to CAα1 were observed in lanes 3 and 4, respectively. In lanes 1 and 2, which contained overexpressed control-GFP adenovirus, and lane 4, faint bands for endogenous AMPKα1 were seen.

Next, the effects on phosphorylation of ACC were examined by Western immunoblotting. As shown in the lower panel of Fig. 1C, forskolin stimulates ACC phosphorylation to an extent similar to that of 2-deoxy-D-glucose. Overexpression of D/Nα1 markedly inhibited ACC phosphorylation as reported previously, while overexpressing the active mutant of AMPK had no significant effect as compared with control GFP.

As shown in Fig. 3B, forskolin treatment induced an approximately 5.5-fold increase in luciferase activity in the CRE-Luc BeWo cells, while neither CAα1 nor D/Nα1 overexpression affected luciferase activity. These results demonstrate that altering AMPK activity does not affect the CRE activity in BeWo cells.

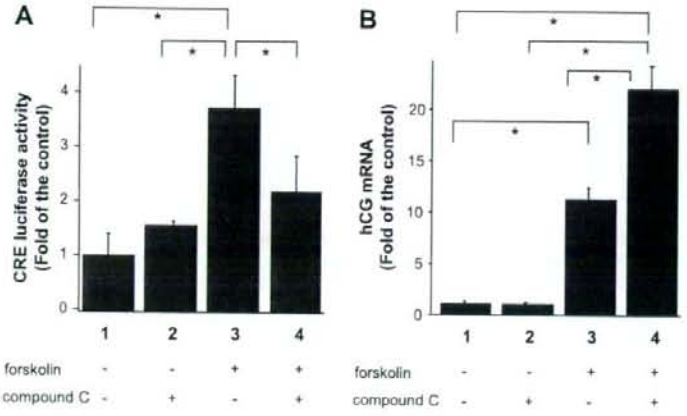

Fig. 2. Forskolin -induced CRE-dependent transcription. A. BeWo cells transfected with a CRE-luciferase reporter construct were treated with vehicle (DMSO), 100 μM forskolin or 10 μM compound C alone or in combination for 1 h as indicated. CRE promoter activity was analysed by luciferase assay. The data presented are means ± SD of three independent experiments. *$p < 0.05$. Culture with DMSO alone served as the control (lane 1). B. hCG mRNAs were analysed using real-time RT-PCR as described in Section 2. The relative levels of mRNA were normalised by β-Actin. Data are means ± SD of at least three independent experiments. *$p < 0.05$.

3.5. Forskolin exerts its effect on TJ assembly via AMPK activation

As shown in Fig. 1A, forskolin treatment promotes TJ assembly in BeWo cells. Thus, we examined whether or not forskolin-induced TJ assembly is mediated by AMPK activation, by immunostaining the ZO-1 cell surface and immunoblotting ZO-1 in Triton-insoluble pools. To inhibit AMPK activity, we used adenoviruses to express D/N AMPK and compound C, a specific inhibitor of AMPK. BeWo cells were pre-transfected with D/Nα1 or control-GFP adenovirus, and incubated with forskolin for 12 h. The cells were collected using the Triton X-100 extractability assay and immunoblotting was carried out. Fig. 4A shows the ZO-1 content of forskolin-treated cells to be larger than that of untreated cells (lanes 1 and 2). In addition, overexpression of D/N AMPK markedly suppressed the forskolin-induced increases in ZO-1 content (lanes 2 and 3). The increase in the amount of ZO-1 induced by 2-deoxy-D-glucose treatment was also inhibited by D/N AMPK, which is in a good agreement with the results of a previous study [12,13,24] (Fig. 4B).

Next, to confirm the effect of forskolin on TJ assembly in BeWo cells, we used a selective AMPK inhibitor, compound C. The increase in ZO-1 on the cell surface in response to forskolin stimulation was shown, by immunostaining using anti-ZO-1 antibody (Fig. 4C), to be blunted by co-incubation with compound C. Similarly, Fig. 4D

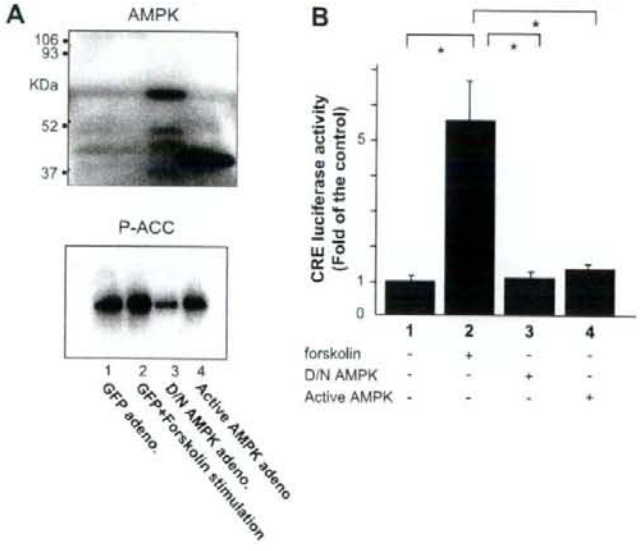

Fig. 3. Expressions of dominant negative and constitutively active forms of AMPKα1 subunit in BeWo cells. A. Western blot analyses of AMPK and phosphorylated ACC were performed as described in Section 2. BeWo cells were transfected with control-GFP adenovirus, D/Nα1 AMPK adenovirus or CAα1 AMPK adenovirus as indicated. Lane2 shows stimulation with 100 μM forskolin alone for 1 h. All adenovirus transfections were carried out for 6 h. B. BeWo cells transfected with a CRE-luciferase reporter construct were additionally transfected and stimulated as shown in the left panel. CRE promoter activity was analysed by luciferase assay. The data presented are means ± SD of three independent experiments. *$p < 0.01$.

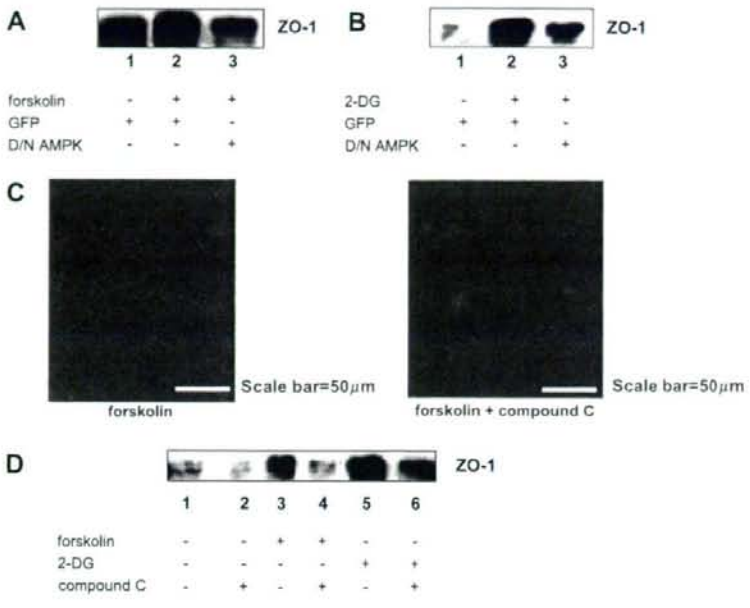

Fig. 4. Effects of forskolin in assembly of TJ strands is exerted via AMPK activation. A. BeWo cells were tranfected with D/Nα1 AMPK adenovirus or control-GFP adenovirus for 6 h and stimulated with 100 μM forskolin for 12 h. Western blotting was performed using anti-ZO-1 antibody. Overexpression of D/Nα1 AMPK adenovirus inhibited the forskolin-induced increases in ZO-1 protein expression. B. BeWo cells were tranfected as in A, and stimulated with 25 mM 2-deoxy-D-glucose for 12 h. 2-Deoxy-D-glucose increased ZO-1 protein expression and this increase was inhibited by D/N AMPK, as in A. C. Immunohistochemical localisation of ZO-1 in BeWo cells. Cells were cultured with 100 μM forskolin or 100 μM forskolin plus 10 μM compound C for 24 h, and stained as in Fig. 1A. Forskolin-induced ZO-1 staining, detected in the cell periphery, was blunted by co-incubation with compound C. D. BeWo cells were treated with 100 μM forskolin, 25 mM 2-deoxy-D-glucose or 10 μM compound C alone or in combination for 12 h as indicated. Western blotting was performed using anti-ZO-1 antibody. Forskolin or 2-deoxy-D-glucose induced increases in ZO-1 protein expression were inhibited by compound C.

presents the results of the Triton X-100 extractability assay and immunoblotting using anti-ZO-1 antibody. The ZO-1 band was increased by 2-deoxy-D-glucose treatment and forskolin, and these effects were inhibited by compound C. Therefore, TJ assembly formation, regardless of whether the induction is by forskolin or 2-deoxy-D-glucose, requires AMPK activation.

3.6. Effect of AMPK activity on forskolin-induced BeWo cell syncytialisation

To determine the effect of AMPK activity on the rate of cell fusion, BeWo cells were cultured in the absence or presence of forskolin alone, forskolin plus AICAR or forskolin plus compound C for 24 h. Then, the number of fused cells was counted using FACS analysis (Fig. 5). Cell fusion was stimulated by the presence of forskolin but no difference was observed between forskolin alone and forskolin plus either AICAR or compound C.

4. Discussion

TJs are directly involved in paracellular sealing (barrier function) as well as in membrane domain differentiation (fence function) [25], and Zonula occludens-1 (ZO-1) is a TJ-associated protein, which acts as a linker between proteins constituting the TJ strands and the actin-based cytoskeleton [26]. TJs are present in normal placenta and are mainly localised in the apical part of the syncytium, in cell–cell contacts between the syncytium and villous cytotrophoblastic cells as well as between cytotrophoblastic cells. Thus, it is likely that TJs contribute to the trophoblastic barrier function of the placenta [8].

The first finding in this study is that forskolin stimulation induces TJ formation in BeWo cells, as clearly demonstrated by immunostaining and immunoblotting of the accumulated ZO-1 in the Triton-insoluble pool. TJ formation is one of the cellular phenomena recently demonstrated to be mediated by AMPK activation [12,13]. AMPK is an intracellular energy sensor and regulator of energy balance at the cellular level. An increased intracellular AMP/ATP ratio leads to a conformational change in AMPK, and AMPK is reportedly activated by any stress that depletes cellular

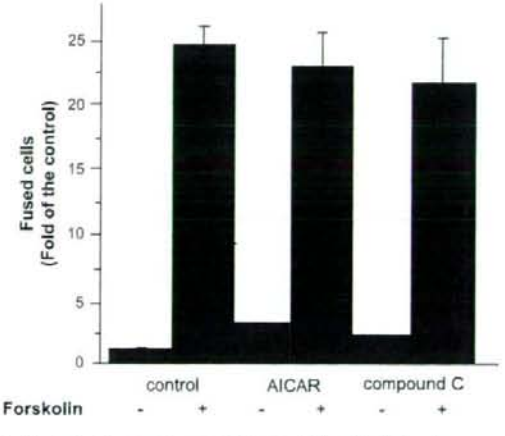

Fig. 5. Effect of AMPK activity on cell-fusion in BeWo cells. BeWo cells expressing either H2B-GFP or Mit-DsRed2 were mixed and cultured with 1 mM AICAR, 10 μM compound C, and vehicle (DMSO) for 2 h. Then, 100 μM forskolin or DMSO was added to the medium and 24 h later, cell fusion was analysed using a FACS as described in Section 2. The data presented are means ± SD of three independent experiments.

ATP, such as nutritional deprivation, ischaemia, hypoxia, oxidative stress and so on [21,27,28]. Indeed, TJ formation by BeWo cells was also observed upon stimulation with AICAR or 2-deoxy-D-glucose, which induces ATP depletion. However, unlike AICAR or 2-deoxy-D-glucose, there are no reports showing forskolin to activate AMPK. Conversely, AMPK activity is reportedly attenuated in response to cAMP-elevating agents and forskolin in INS-1, mouse embryonic fibroblasts, and COS cells [29]. Phosphorylations at Ser485 and Ser491 of the α1 and α2 subunits, respectively, were suggested to be involved in the kinase activity attenuation by forskolin, while phosphorylation of the α-Thr172 residue leading to kinase activation is reduced via inhibition of calcium/calmodulin-dependent protein kinase kinase-α/β. Thus, we investigated the effect of forskolin on AMPK in BeWo cells, and found that AMPK is activated by long-term, but not by short-term stimulation, forskolin stimulation. The phosphorylations of Thr172 of AMPK, a subunit, and one of its cellular substrates, ACC, were both observed. Such phosphorylations increases did not occur until at least 8 h of forskolin stimulation (data not shown). Since we used the antibody recognising phospho-Ser79 specific antibody, the ACC phosphorylation observed in our study was attributable to AMPK activation, not to PKA activation. In addition, these phosphorylations were inhibited by the AMPK inhibitor compound C or overexpression of the dominant negative AMPKα subunit. It was also shown that compound C or overexpression of the dominant negative AMPKα subunit inhibited forskolin-induced TJ formation. Since compound C does not inhibit hCG gene expression, which is reportedly mediated by CRE activity, it seems that the PKA-CRE transcriptional activation pathway is not important for forskolin-induced TJ formation. Based on these findings, it was concluded that AMPK activation is necessary for forskolin-induced TJ formation in BeWo cells. In contrast, forskolin-induced cell fusion of BeWo cells was not affected by AICAR or compound C, suggesting that the AMPK pathway is not involved in cell fusion. It also means that TJ formation and cell fusion take place via independent mechanisms, although both can be induced by forskolin.

It is possible that, with partial and complete moles, which are characterised by hydropic villi, the early loss of or alterations in TJ integrity are related to phenotypic changes. Since TJs localised not only in the syncytium but also in placental endothelial vessels, altered TJ formation in fetal vessels may increase permeability and contribute to the formation of hydropic villi [8]. Furthermore, alterations of TJ components are reportedly related to preeclampsia [30].

Although much remains unclear as to how syncytialised cells which cover the chorionic villi form the barrier comprised of TJ, our results suggest that AMPK is activated not only by nutrients or ATP deficiency but also various hormones or factors increasing cAMP contents, such as forskolin, and thereby plays an important role. Though further study is needed to elucidate the molecular mechanism underlying long-term forskolin-induced AMPK activation, this is the first report providing evidence that AMPK is involved in long-term stimulation with forskolin. This mechanism may also be important for normal placental development. Another important question involves the relationship between cellular energy status and syncytialisation. Determining the mechanism of TJ formation, we might allow clarification of the pathology of incomplete placentation, especially incomplete TJ formation.

Acknowledgements

This work was carried out at the Analysis Center of Life Science, Hiroshima University.

References

[1] Farquhar MG, Palade GE. Junctional complexes in various epithelia. J Cell Biol 1963;17:375–412.
[2] Anderson JM, Van Itallie CM, Fanning AS. Setting up a selective barrier at the apical junction complex. Curr Opin Cell Biol 2004;16:140–5.
[3] Balda MS, Matter K. Tight junctions. J Cell Sci 1998;111(Pt 5):541–7.
[4] Tsukita S, Furuse M, Itoh M. Multifunctional strands in tight junctions. Nat Rev Mol Cell Biol 2001;2:285–93.
[5] Schneeberger EE, Lynch RD. The tight junction: a multifunctional complex. Am J Physiol Cell Physiol 2004;286:C1213–28.
[6] Huber JD, Egleton RD, Davis TP. Molecular physiology and pathophysiology of tight junctions in the blood–brain barrier. Trends Neurosci 2001;24:719–25.
[7] Benirschke K, Kaufman P. Pathology of the human placenta. 4th ed. Springer; 2000. 65-72 pp.
[8] Marzioni D, Banita M, Felici A, Paradinas FJ, Newlands E, De Nictolis M, et al. Expression of ZO-1 and occluding in normal human placenta and in hydatidiform moles. Mol Hum Reprod 2001;7(3):279–85.
[9] Pattillo RA, Gey GO, Delfs E, Mattingly RF. Human hormone production in vitro. Science 1968;159:1467–9.
[10] Ringler GE, Strauss 3rd JF. In vitro systems for the study of human placental endocrine function. Endocr Rev 1990;11:105–23.
[11] Strauss 3rd JF, Kido S, Sayegh R, Sakuragi N, Gafvels ME. The cAMP signalling system and human trophoblast function. Placenta 1992;13:389–403.
[12] Zhang L, Li J, Young LH, Caplan MJ. AMP-activated protein kinase regulates the assembly of epithelial tight junctions. Proc Natl Acad Sci USA 2006;103:17272–7.
[13] Zheng B, Cantley LC. Regulation of epithelial tight junction assembly and disassembly by AMP-activated protein kinase. Proc Natl Acad Sci USA 2007;104:819–22.
[14] Stein SC, Woods AC, Jones NA, Davison MD, Carling D. The regulation of AMP-activated protein kinase by phosphorylation. Biochem J 2000;345(Pt 3):437–43.
[15] Pasdar M, Nelson WJ. Kinetics of desmosome assembly in Madin–Darby canine kidney epithelial cells: temporal and spatial regulation of desmoplakin organization and stabilization upon cell–cell contact. I. Biochemical analysis. J Cell Biol 1988;106:677–85.
[16] Stuart RO, Sun A, Bush KT, Nigam KS. Dependence of epithelial intercellular junction biogenesis on thapsigargin-sensitive intracellular calcium stores. J Biol Chem 1996;271:13636–41.
[17] Kudo Y, Boyd CAR, Kimura H, Cook PR, Redman CWG, Sargent IL. Quantifying the syncytialisation of human placental trophoblast BeWo cells grown in vitro. Biochim Biophys Acta 2003;1640:25–31.
[18] Stevenson BR, Siliciano JD, Mooseker MS, Goodenough DA. Identification of ZO-1: a high molecular weight polypeptide associated with the tight junction (zonula occludens) in a variety of epithelia. J Cell Biol 1986;103:755–66.
[19] Anderson JM, Stevenson BR, Jesaitis LA, Goodenough DA, Mooseker MS. Characterization of ZO-1, a protein component of the tight junction from mouse liver and Madin–Darby canine kidney cells. J Cell Biol 1988;106:1141–9.
[20] Hardie DG, Scott JW, Pan DA, Hudson ER. Management of cellular energy by the AMP-activated protein kinase system. FEBS Lett 2003;546:113–20.
[21] Zhu Z, Jiang W, McGinley JN, Thompson HJ. 2-Deoxyglucose as an energy restriction mimetic agent: effects on mammary carcinogenesis and on mammary tumor cell growth in vitro. Cancer Res 2005;65:7023–30.
[22] Feinman MA, Kliman HJ, Caltabiano S, Strauss 3rd JF. 8-Bromo-3′, 5′-adenosine monophosphate stimulates the endocrine activity of human cytotrophoblasts in culture. J Clin Endocrinol Metab 1986;63:1211–7.
[23] Woods A, Azzout-Marniche D, Foretz M, Stein SC, Lemarchand P, Ferre P, et al. Characterization of the role of AMP-activated protein kinase in the regulation of glucose-activated gene expression using constitutively active and dominant negative forms of the kinase. Mol Cell Biol 2000;20:6704–11.
[24] Forcet C, Billaud M. Dialogue between LKB1 and AMPK: a hot topic at the cellular pole. Sci STKE 2007;404:pe51.
[25] Tsukita S, Furuse M. Occludin and claudins in tight-junction strands: leading or supporting players? Trends Cell Biol 1999;9:268–73.
[26] Gonzalez-Mariscal L, Betanzos A, Avila-Flores A. MAGUK proteins: structure and role in the tight junction. Semin Cell Dev Biol 2000;11:315–24.
[27] Vavvas D, Apazidis A, Saha AK, Gamble J, Patel A, Kemp BE, et al. Contraction-induced changes in acetyl-CoA carboxylase and 5′-AMP-activated kinase in skeletal muscle. J Biol Chem 1997;272:13255–61.
[28] Hayashi T, Hirshman MF, Kurth EJ, Winder WW, Goodyear LJ. Evidence for 5′AMP-activated protein kinase mediation of the effect of muscle contraction on glucose transport. Diabetes 1998;47:1369–73.
[29] Hurley RL, Barre LK, Wood SD, Anderson KA, Kemp BE, Means AR, et al. Regulation of AMP-activated protein kinase by multisite phosphorylation in response to agents that elevate cellular cAMP. J Biol Chem 2006;281:36662–72.
[30] Lievano S, Alarcon L, Chavez-Munguia B, Gonzalez-Mariscal L. Endothelia of term human placentae display diminished expression of tight junction proteins during preeclampsia. Cell Tissue Res 2006;324:433–48.

THE JOURNAL OF BIOLOGICAL CHEMISTRY VOL. 283, NO. 49, pp. 33902–33910, December 5, 2008

AMP-activated Protein Kinase Activation Increases Phosphorylation of Glycogen Synthase Kinase 3β and Thereby Reduces cAMP-responsive Element Transcriptional Activity and Phosphoenolpyruvate Carboxykinase C Gene Expression in the Liver*[S]

Received for publication, April 2, 2008, and in revised form, September 17, 2008 Published, JBC Papers in Press, September 17, 2008, DOI 10.1074/jbc.M802537200

Nanao Horike[‡], Hideyuki Sakoda[§], Akifumi Kushiyama[¶], Hiraku Ono[§], Midori Fujishiro[§], Hideaki Kamata[‖], Koichi Nishiyama[‡], Yasunobu Uchijima[‡], Yukiko Kurihara[‡], Hiroki Kurihara[‡], and Tomoichiro Asano[‖1]

From the [‡]Department of Physiological Chemistry and Metabolism, Graduate School of Medicine, University of Tokyo, 7-3-1 Hongo, Bunkyo-ku, Tokyo, [§]Department of Internal Medicine, Graduate School of Medicine, University of Tokyo, 7-3-1 Hongo, Bunkyo-ku, Tokyo, [¶]Institute for Adult Disease, Asahi Life Foundation, Tokyo, and [‖]Department of Medical Science, Graduate School of Medicine, University of Hiroshima, 1-2-3 Kasumi, Minami-ku, Hiroshima City, Hiroshima, Japan 734-8553

AMP-activated protein kinase (AMPK) activation reportedly suppresses transcriptional activity of the cAMP-responsive element (CRE) in the phosphoenolpyruvate carboxykinase C (PEPCK-C) promoter and reduces hepatic PEPCK-C expression. Although a previous study found TORC2 phosphorylation to be involved in the suppression of AMPK-mediated CRE transcriptional activity, we herein present evidence that glycogen synthase kinase 3β (GSK3β) phosphorylation induced by AMPK also plays an important role. We initially found that injecting fasted mice with 5-aminoimidazole-4-carboxamide ribonucleoside (AICAR) markedly increased Ser-9 phosphorylation of hepatic GSK3β within 15 min. Stimulation with AICAR or the GSK3β inhibitor SB-415286 strongly inhibited CRE-containing promoter activity in HepG2 cells. Using the Gal4-based transactivation assay system, the transcriptional activity of cAMP-response element-binding protein (CREB) was suppressed by both AICAR and SB415286, whereas that of TORC2 was repressed significantly by AICAR but very slightly by SB415286. These results show inactivation of GSK3β to directly inhibit CREB but not TORC2. Importantly, the AICAR-induced suppression of PEPCK-C expression was shown to be blunted by overexpression of GSK3β(S9G) but not wild-type GSK3β. In addition, AICAR stimulation decreased, whereas Compound C (AMPK inhibitor) increased CREB phosphorylation (Ser-129) in HepG2 cells. The time-courses of decreased CREB phosphorylation (Ser-129) and increased GSK3β phosphorylation were very similar. Furthermore, AMPK-mediated GSK3β phosphorylation was inhibited by an Akt-specific inhibitor in HepG2 cells, suggesting involvement of the Akt pathway. In summary, phosphorylation (Ser-9) of GSK3β is very likely to be critical for AMPK-mediated PEPCK-C gene suppression. Reduced CREB phosphorylation (Ser-129) associated with inactivation of GSK3β by Ser-9 phosphorylation may be the major mechanism underlying PEPCK-C gene suppression by AMPK-activating agents such as biguanide.

Hepatic PEPCK-C[2] expression plays a critical role in the maintenance of glucose homeostasis, and activation of AMPK in the livers of fasted mice has been shown to reduce glucose production (1). The oral biguanide antidiabetic agent metformin and several factors including leptin and adiponectin reportedly activate AMPK, improve insulin sensitivity, and reduce gluconeogenesis in patients with type 2 diabetes mellitus (2–8). It was also reported that stimulation with the AMPK activator 5-aminoimidazole-4-carboxamide ribonucleoside (AICAR) suppresses hepatic PEPCK-C expression and the transcriptional activity of the cAMP-responsive element (CRE), which is present in the PEPCK-C promoter, actions similar to those of insulin (9).

AMPK achieves its downstream effects by immediate direct phosphorylation of enzyme substrates as well as long term effects on gene expression. For example, AMPK phosphorylates and inactivates acetyl-CoA carboxylase, resulting in suppression of the conversion of acetyl CoA to malonyl CoA (4). This malonyl CoA reduction allows entry of fatty acids into mitochondria and their subsequent oxidation (10, 11). Recently, as a molecular mechanism underlying AMPK-mediated PEPCK-C gene suppression, the phosphorylation of TORC2 (transducer of regulated CREB activity 2), a co-activator of cAMP-responsive element binding (CREB) protein, by AMPK was reported (12–15). TORC2 phosphorylated by AMPK or SIK binds to 14-3-3, and this complex is transported

* The costs of publication of this article were defrayed in part by the payment of page charges. This article must therefore be hereby marked "*advertisement*" in accordance with 18 U.S.C. Section 1734 solely to indicate this fact.

[S] The on-line version of this article (available at http://www.jbc.org) contains supplemental Fig. 1.

[1] To whom correspondence should be addressed: Dept. of Medical Science, Graduate School of Medicine, University of Hiroshima, 1-2-3 Kasumi, Minami-ku, Hiroshima City, Hiroshima, Japan 734-8553. Tel.: 81-82-257-5135; Fax: 81-82-257-5136; E-mail: asano-tky@umin.ac.jp.

[2] The abbreviations used are: PEPCK-C, phosphoenolpyruvate carboxykinase C; GSK3β, glycogen synthase kinase 3β; AMPK, AMP-activated protein kinase; AICAR, 5-aminoimidazole-4-carboxamide ribonucleoside; CREB, CRE, cAMP-response element; CREB, CRE-binding protein; TORC2, transducer of regulated CREB activity 2; WT, wild type; GST, glutathione S-transferase; CBP, CREB-binding protein; UAS, upstream activating sequence; ACC, acetyl-CoA carboxylase; SIK, salt-inducible kinase.

from inside the nucleus to the cytoplasm (16, 17). Thus, by reducing the association with TORC2 and CREB in the nucleus, CRE transcriptional activity and PEPCK-C expression are suppressed.

On the other hand, it has been revealed that CRE transcriptional activity is regulated not only by nuclear TORC2 but also by the phosphorylation of CREB. For example, forskolin stimulates cAMP production and enhances PEPCK-C gene expression by stimulating the protein kinase A-mediated phosphorylation of CREB at Ser-133 and by promoting subsequent recruitment of the coactivator CREB-binding protein (CBP) to the promoter (18, 19). Furthermore, CREB has been regarded as one of the potential nuclear substrates of GSK3β, which were identified by *in vitro* phosphorylation and overexpression studies (20–22). Thus, it has been suggested that GSK3β phosphorylates CREB at Ser-129, leading to a stimulatory effect on CREB activity, and that CREB is involved in the cAMP-mediated activation of PEPCK-C expression (22–24). Because Akt/protein kinase B phosphorylates and inactivates GSK3β, insulin-induced suppression of CRE transcriptional activity is likely to be mediated by Akt-induced GSK3β phosphorylation at Ser-129. The phosphorylations of either CREB or TORC2 could,, thus, regulate transcriptional activity and thereby the gene expression of PEPCK-C.

In this study we observed that AMPK activation increases GSK3β phosphorylation rapidly and markedly in the mouse liver. Then, we performed experiments to determine whether AMPK-induced PEPCK-C gene suppression is indeed mediated by increased GSK3β phosphorylation. Herein, we present evidence showing a critical role of GSK3β phosphorylation in the AMPK-induced suppression of hepatic gluconeogenesis.

EXPERIMENTAL PROCEDURES

Reagents—AMPK inhibitor Compound C and Akt inhibitor IV were purchased from Calbiochem. Phospho-ACC (Ser-79), phospho-Akt (Thr-308), and phospho-GSK3β(Ser-9) antibodies were purchased from Cell Signaling Technology (Beverly, MA). Anti-rabbit horseradish peroxidase antibodies conjugated to horseradish peroxidase were obtained from Amersham Biosciences. Dulbecco's modified Eagle's medium and fetal bovine serum were purchased from Invitrogen. All other reagents were of analytical grade. A rabbit polyclonal antibody was raised against a SIK(C) fragment (amino acid residues 1–343) or TORC2 peptide (563–699) in rabbits as described previously (25).

Preparation of Tissue Extracts—After an overnight fast or injection of AICAR (250 mg/kg), the animal was killed by cervical dislocation before removal of the liver. One part of the liver was homogenized in 10 volumes of ice-cold lysis buffer (20 mM Tris-HCl, pH 8.0, 1% Triton, 1 mM EDTA, 1 mM EGTA, 1 mM sodium orthovanadate, 1 mM dithiothreitol, 1 mM phenylmethylsulfonyl fluoride, and 2 μg/ml leupeptin). The solution was then centrifuged at 10,000 $\times$ *g* at 4 °C. The supernatant was collected, and the protein concentration was measured using a Bio-Rad protein assay kit.

Cell Culture—Human hepatoma HepG2 cells were obtained from the American Type Culture Collection (Manassas, VA). HepG2 cells were cultured in Dulbecco's modified Eagle's medium containing 10% fetal bovine serum, 100 units/ml penicillin, 100 μg/ml streptomycin, and 5.5 mM D-glucose. The cells were incubated in a humidified atmosphere of 5% CO_2 at 37 °C and passaged every 3 days by trypsinization. Primary hepatocytes were isolated from male C57B6 mice by the collagenase method. Cells were suspended in William's E medium (Sigma) containing 10% fetal bovine serum, 1 nM insulin, 75 mg/liter penicillin, and 50 mg/liter streptomycin and then plated. After 12 h, serum was removed, and the cells were divided into control or dexamethasone (1 μM) groups. The medium was the same as that described above except that 0.1% bovine serum albumin was added instead of fetal bovine serum.

Construction and Luciferase Assay—The following plasmids were obtained from commercial sources: pTAL, pTAL-CRE and pM from Clontech (Palo Alto, CA) and pGL4.10 and pRL-TK from Promega (Madison, WI). The PEPCK-C promoter (−450 to −1) was inserted into a pGL4.10 vector (Promega). HepG2 cells in a 12-well collagen-coated plate were cotransfected with PEPCK-C-LUC vector (0.5 μg/well) with an internal reporter, pRL-TK (0.03 μg). For the CREB or TORC2 reporter assay, cells were transformed with Gal4 DNA binding domain-linked CREB expression vectors (pM-CREB, pM-TORC2, or pM, empty vector, 0.15 μg) and reporter vectors (UAS-linked luciferase reporter (pTAL-5x UAS, 0.15 μg) and an internal reporter, pRL-TK (0.03 μg)). pM was used to express a fusion protein that possessed the GAL4 DNA binding domain at the N terminus of a protein of interest. The fusion protein was transported into the nucleus by the SV40 nuclear localization sequence created in the GAL4 DNA binding domain. The luciferase reporter construct containing five copies of the GAL4 DNA binding site (UAS) upstream from the c-*fos* minimal promoter (FR-luc) was obtained from Stratagene. Because luciferase activity derived from FR-luc was low, the BamHI/XbaI fragment containing five copies of UAS elements of FR-Luc was transferred to the BglII/NheI site of pTAL, and the resultant reporter was named pTAL-5× UAS(26). After 48 h of transfection, cells were treated with or without forskolin (10 μM) or AICAR (2 mM) for 6 h and harvested to measure luciferase activities by the Dual-luciferase Reporter Assay System (Promega Corp.). Specific promoter activities of PEPCK-C, CRE, CREB, or TORC2 genes were expressed as -fold expression compared with the reporter activity of the empty vector. Luciferase activities were measured and normalized by *Renilla* luciferase activity.

Site-directed Mutagenesis and Generation of Recombinant Adenovirus—Ser-9 of the wild-type GSK3β construct was mutated to a glycine to generate the GSK3β-S9G mutant construct using site-directed mutagenesis. Template DNA (5 ng) was mixed with 20 pmol of each primer (GSK3β-S9G: forward primer, 5′-ACCACCGCCTTTGGCGAGAGCTG-3′; GSK3β-S9G reverse primer, 5′-CAGCTCTCGCCAAAGGCGGTGGT-3′), and the PCR was run (94 °C, 30 s; 55 °C, 1 min; 68 °C, 5 min; 12 cycles). The product was transformed into DH5α competent *Escherichia coli*. Recombinant adenoviruses used to express wild-type GSK3β(WT) and constitutive active GSK3β(S9G) were constructed by homologous recombination of the expression cosmid cassettes containing the correspond-

ing cDNAs and the parental virus genome, as described previously (27).

Adenoviral Gene Transfer—Recombinant adenovirus expressing wild-type and dominant negative mutant forms of AMPKα, wild-type GSK3β(WT), SIK1 and constitutive active GSK3β(S9G) were generated, purified, and concentrated using cesium chloride ultracentrifugation as reported previously (27). Adenovirus encoding LacZ served as a control, and the adenoviral gene transfer was performed as reported previously (27).

Western Blot Analysis—Western blot analysis was carried out as described previously (27). In brief, HepG2 cells were lysed in lysis buffer as shown above. Cell debris was removed by centrifugation at 12,000 $\times$ *g* for 15 min at 4 °C, and the resulting supernatant (cell lysate) was used for Western blotting and lipid content analysis. For Western blotting, 10 μg of protein were separated by 12% SDS-PAGE and electrophoretically transferred to polyvinylidene difluoride membranes in a transfer buffer consisting of 20 mM Tris-HCl, 150 mM glycine, and 20% methanol. The membranes were blocked with 5% nonfat dry milk in Tris-buffered saline with 0.1% Tween 20 and incubated with specific antibodies followed by incubation with horseradish peroxidase-conjugated secondary antibodies. The antigen-antibody interactions were visualized by incubation with ECL chemiluminescence reagent (Amersham Biosciences).

Immunoprecipitations—For the immunoprecipitation experiments, HepG2 cells were transfected with 1 μg of GST-tagged CREB. Whole-cell extracts were prepared from HepG2 cells in lysis buffer, as described above. Cell extracts were incubated for 4 h at 4 °C with anti-GST antibody (5 μg) and then for 1 h with 30 μl of protein G-Sepharose beads. The pellets were washed 5 times with 1 ml of lysis buffer, then resuspended in Laemmli sample buffer, boiled for 3 min, and analyzed on SDS/8% polyacrylamide gels.

RESULTS

AICAR Stimulation Increases the Phosphorylations of GSK3β and ACC in Mouse Liver—AICAR was intraperitoneally injected into fasted mice, and the Ser-9 phosphorylation level of hepatic GSK3β was monitored at the indicated times (Fig. 1). As reported previously, AICAR stimulation increased ACC phosphorylation (*lowest panel* of Fig. 1). Interestingly, GSK3β phosphorylation was also markedly increased by AICAR injection, whereas the level of GSK3β protein expression was unchanged in the livers of fasted mice. This increase took place within 15 min of injecting AICAR, peaked at 30 min, and persisted for 2 h. Thus, AICAR stimulation was revealed to enhance not only ACC but also GSK3β, probably more markedly than ACC.

AMPK Activation Reduces Transcriptional Activities of PEPCK-C Gene Promoter and CRE—PEPCK-C regulation *in vivo* occurs mainly at the level of gene expression (28–32). Expression of the luciferase gene located downstream from the PEPCK-C gene promoter was markedly increased by forskolin in HepG2 cells, and this increase was suppressed by AICAR or insulin stimulation (Fig. 2*A*). Because the domain responsible for the forskolin-induced PEPCK-C up-regulation is reportedly that of CRE, we subsequently performed a luciferase assay using a plasmid containing the CRE domain upstream from the luciferase gene (Fig. 2*B*). Forskolin markedly enhanced CRE transcriptional activity, whereas AICAR almost completely abolished it, and the AMPK inhibitor Compound C had no effect. Interestingly, the GSK3β inhibitor SB415286 also very strongly inhibited the forskolin-induced increase in CRE activity (Fig. 2*B*). Furthermore, to confirm that the effect of AICAR is mediated by increased AMPK activity, the wild-type and dominant negative mutant of AMPK were overexpressed, employing adenovirus-mediated gene transfer. The overexpressed proteins were detected by immunoblotting (*upper blot* in the *right panel* of Fig. 2*C*). As predicted, AMPK overexpression increased ACC phosphorylation, whereas a dominant negative form suppressed it (*lower blot* in the *right panel* of Fig. 2*C*). Under these conditions, AMPK was revealed to suppress forskolin-induced CRE transcriptional activity (*left panel* of Fig. 2*C*).

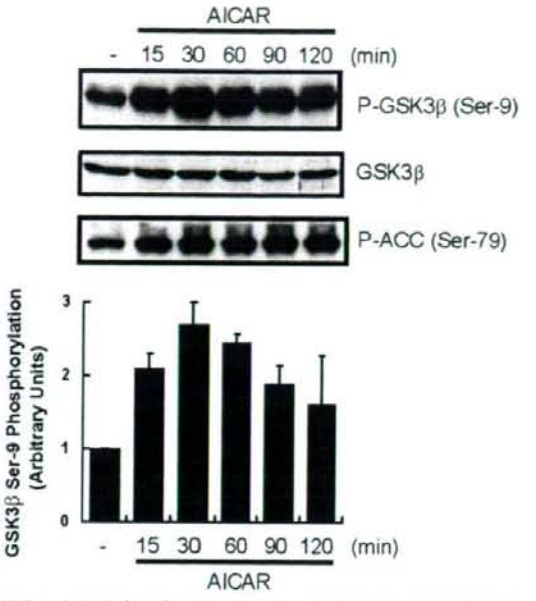

FIGURE 1. **AICAR induced GSK3β phosphorylation in livers of fasted mice.** Ten-week-old C57BL6 mice were fasted overnight, then given an intraperitoneal injection of AICAR (250 mg/kg) before sacrifice followed by excision of the liver. Ser-9 phosphorylation (*P-*) of GSK3β was assessed by Western blotting. The phospho-GSK3β was quantified densitometrically, and the results are presented in the *lower panel*. The results are presented as the mean ± S.E. of three independent experiments.

Contribution of CREB and TORC2 in the AMPK-, SIK1-, and GSK3β-mediated Suppression of CRE Activity—Because both AICAR and SB415286 repressed CRE-dependent reporter activity (Fig. 2*B*), we performed the experiments to determine which of these molecules (CREB or TORC2) is involved in the AICAR- and SB415286-induced suppression of the CRE transcriptional activity, using a GAL4-based transactivation assay system in HepG2 cells. Expression vectors encoding the DNA binding domain of the yeast transcription factor GAL4 fused to CREB were co-transfected with a GAL4-binding site (UAS)-driven luciferase reporter gene. To eliminate the interaction between the bZIP domain of CREB and the N-terminal coiled-coil region of TORC2, the transactivation domains of CREB and TORC2 were separated from the bZIP domain and the

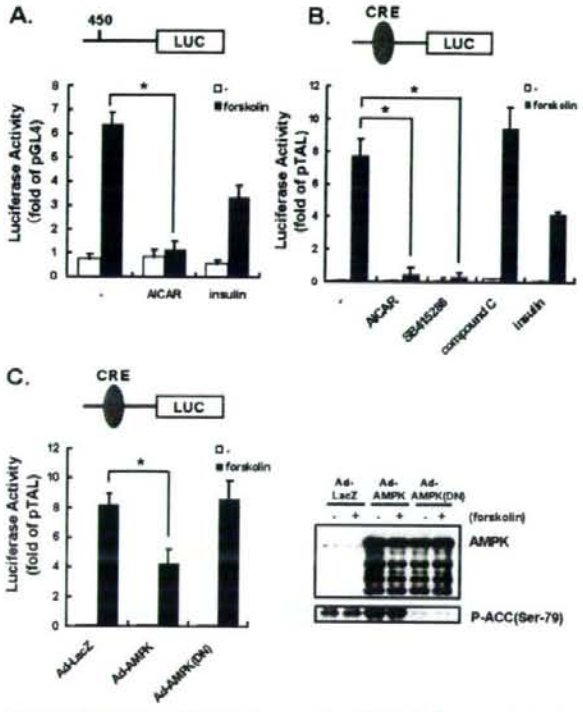

FIGURE 2. **Inhibition of PEPCK-C reporter by AICAR in HepG2 cells in the presence and the absence of forskolin.** AICAR or the GSK3β inhibitor SB-415286 has the potential to down-regulate CRE-dependent transcription in the presence and in the absence of 10 μM forskolin. HepG2 cells were transfected with the PEPCK-C promoter fused to the luciferase reporter plasmid (pGL4.10-PEPCK-C: 0.5 μg) with an internal reporter, pRL-TK (0.03 μg). HepG2 cells were serum-starved overnight before incubation with AICAR (2 mM) or insulin (10 nM) with or without 10 μM forskolin. After a 6-h incubation, cells were harvested for the reporter assay. *A*, the PEPCK-C-dependent reporter activities that had been normalized with internal reporter activities were expressed as -fold activities of the empty reporter (pGL4.10). *B*, HepG2 cells were transfected with the CRE-reporter plasmid (pTAL-CRE: 0.25 μg) with the internal reporter pRL-TK (0.03 μg). HepG2 cells were serum-starved overnight before incubation with AICAR (2 mM), insulin (10 nM), the selective AMPK inhibitor Compound C (20 μM), GSK3β inhibitor, or SB-415286 (30 μM) with or without 10 μM forskolin. After a 6-h incubation, cells were harvested for the reporter assay. *C*, AMPK (WT, DN) was overexpressed by adenoviral (*Ad*) gene transfer, and expressions were detected by anti-AMPK antibody (*upper blot in the right panel*). AMPK activity was monitored by antiphospho-Ser79-ACC (*lower blot in the right panel*). The cells were transfected with the CRE-reporter plasmid (pTAL-CRE, 0.25 μg) with the internal reporter pRL-TK (0.03 μg), and the reporter assay was performed.

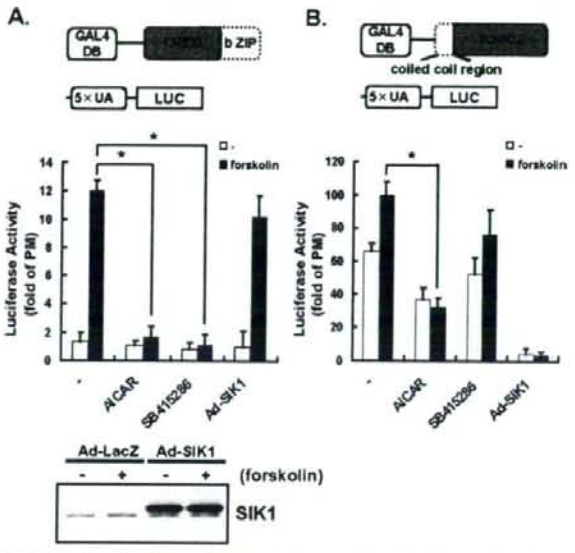

FIGURE 3. **Contributions of CREB and TORC2 to AMPK-, SIK1-, and GSK3β-mediated suppressions of CRE activity.** HepG2 cells were cotransfected with the expression plasmids for GAL4-truncated CREB (bZIP domain) (0.25 μg) or GAL4-truncated TORC2 (coiled coil region) (0.25 μg) and a pTAL-5× UAS reporter plasmid (0.25 μg) with the internal reporter pRL-TK (0.03 μg) (*A* and *B*). HepG2 cells were serum-starved overnight before incubation with AICAR (2 mM), insulin (10 nM), and GSK3β inhibitor or SB-415286 (30 μM) with or without 10 μM forskolin. Adenovirus (*Ad*)-mediated overexpressions of SIK1 proteins were detected using an anti-SIK1 immunoblot (*lower panel*). The specific transactivation activities of TORCs were expressed as the -fold activation of the empty Gal4 vector, pM. Means and S.D. are indicated ($n = 3$). *, $p < 0.05$.

N-terminal coiled-coil region, respectively (*upper diagram* of Fig. 3, *A* and *B*). This allowed investigation of the transactivation potential of the transcription factor, independently of its DNA binding and endogenous background.

As shown in Fig. 3*A*, the transcriptional activity of CREB was inhibited by both AICAR and SB415286, whereas that of TORC2 was repressed by AICAR significantly and by SB415286 slightly. These results suggested that AMPK might inhibit the activities of both CREB and TORC2, whereas GSK-3β might up-regulate the activity of only CREB. The zero effect of SB415286 on the level of phosphorylation of TORC2 (Fig. 4) might also support this hypothesis.

On the other hand, TORC2 is known to be highly phosphorylated and inactivated by SIK1, a member of the AMPK family of Ser/Thr kinases. SIK1 phosphorylates TORC2 and blocks its nuclear accumulation (16). Indeed, when SIK1 was overexpressed, the forskolin-induced increase in GAL4-TORC2 activity was completely abolished (Fig. 3*B*). In addition, TORC2 was strongly phosphorylated in adenovirus-expressing SIK1 (*Ad-SIK1*) cells (Fig. 4*B*). Thus, as shown with the GAL4-system and phosphorylation-dependent mobility shift of TORC2, CREB appears to be crucial for exerting the effects of SB415286 and AICAR, whereas TORC2 appears to be crucial for manifestation of the effects of AICAR stimulation and SIK overexpression.

Phosphorylation of TORC2 and ACC by AMPK and SIK1—AMPK and SIK1 reportedly phosphorylate TORC2 (Ser-171), and phosphorylated TORC2 is transported from within the nucleus to the cytoplasm (12). As shown in Fig. 4, endogenous hepatic TORC2 was markedly dephosphorylated upon stimulation with forskolin (*lanes 1* and *2* of Fig. 4, *A* and *B*). Stimulation of hepatocytes with AICAR resulted in a slight shift in the mobility of TORC2, indicating phosphorylation (*lanes 1* and *5* or *lanes 2* and *6* of Fig. 4*A* and *lanes 1* and *3* or *lanes 2* and *4* of Fig. 4*B*), whereas stimulation with a GSK3β specific inhibitor, SB415286, did not produce a shift in response to the presence or absence of forskolin (*lanes 3* and *4* of Fig. 4*A*). On the other hand, TORC2 was strongly phosphorylated in adenovirus-expressing SIK1 (Ad-SIK1) cells (*bottom panel* of Fig. 4*B*), *i.e.* more than with AICAR stimulation (*lanes 5* and *6* of Fig. 4*B*). These results suggest that whereas AICAR stimulation induces

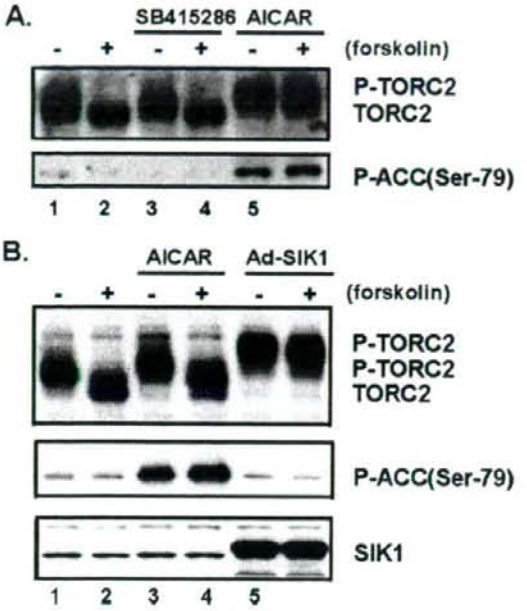

FIGURE 4. **Effect of GSK3β inhibitor SB-415286-, AICAR-, or adenovirus-expressed SIK1 (Ad-SIK1) on P-TORC2 levels in primary hepatocytes in the presence and the absence of forskolin.** *A*, stimulation of hepatocytes with GSK3β inhibitor, SB415286, did not shift the mobility of TORC2 in response to the presence or absence of forskolin. Primary hepatocytes were serum-starved overnight before a 2-h incubation with 30 μM SB-415286 (*lanes 3* and *4*) or 2 mM AICAR (*lanes 5* and *6*) with or without 10 μM forskolin. TORC2 phosphorylation was detected by Western blotting as a phosphorylation-dependent mobility shift (TORC2, dephosphorylated; P-TORC2, phosphorylated) in primary hepatocytes. AMPK activity was monitored by antiphospho-Ser-79-ACC (*lower panel*). *B*, TORC2 was strongly phosphorylated in adenovirus-expressing SIK1. Primary hepatocytes were stimulated with 2 mM AICAR (*lanes 3* and *4*) and adenovirus-mediated overexpressions of SIK1(*lanes 5* and *6*) with or without 10 μM forskolin. AMPK activity was monitored by antiphospho-Ser-79-ACC (*middle panel*). SIK1 proteins were detected using an anti-SIK1 immunoblot (*lower panel*). Data are representative of at least three independent experiments.

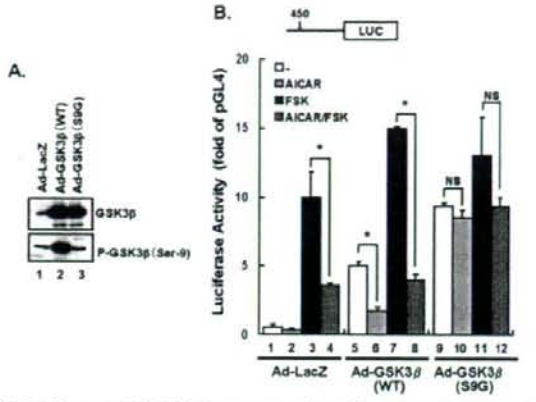

FIGURE 5. **Mutant GSK3β(S9G) overexpression affects PEPCK-C transcriptional activity in HepG2 cells.** HepG2 cells were transiently transfected with pGL4.10-PEPCK-C (0.5 μg) with the internal reporter pRL-TK (0.03 μg). After 5 h of transfection, HepG2 cells were infected with LacZ, GSK3β(WT), or GSK3β(S9G) adenovirus. After 48 h of transfection, the cells were stimulated with or without 2 mM AICAR or 10 μM forskolin for 6 h. *A*, adenovirus-mediated overexpression of GSK3β(WT, S9G) was detected by anti-GSK3β antibody or anti-phospho-(*P*-)Ser-9-GSK3β. *B*, the cells were incubated in the presence and in the absence of 2 mM AICAR or 10 μM forskolin, and the reporter assays were then performed. The results are presented as mean relative luciferase (*LUC*) units (±S.E.), normalized to *Renilla* LUC activity, derived from three independent experiments. *, $p < 0.05$.

TORC2 phosphorylation, SIK1 is likely to phosphorylate more serine residues than AMPK. In contrast, ACC was phosphorylated by AICAR but not by SIK1 (*middle panel* of Fig. 4*B*).

Active Mutant of GSK3β Inhibits AICAR-induced Suppression of Transcriptional Activity of PEPCK-C Promoter—Phosphorylation of GSK3β on Ser-9 inhibits its catalytic activity. In examining whether AICAR-induced suppression of the PEPCK-C gene occurs via GSK3β phosphorylation, we created non-phosphorylatable, constitutively active mutants of the GSK3β(S9G) and GSK3β(WT) adenoviruses. Western blots of total extracts from infected cells treated for 48 h revealed marked overexpressions of GSK3β(S9G) and GSK3β(WT) compared with endogenously expressed GSK3β (*upper panel* of Fig. 5*A*). Furthermore, GSK3β(WT) was detected by anti-phospho-Ser-9 GSK3β antibody, whereas GSK3β(S9G) was not (*lower panel* of Fig. 5*A*). HepG2 cells were incubated with 1.4×10^8 plaque-forming units/well (12-well plate) of adenovirus particles in Dulbecco's modified Eagle's medium. Infection of HepG2 cells with an adenovirus-expressing GSK3β produced a 10–20-fold increase.

In control-LacZ-overexpressing HepG2 cells, forskolin enhances PEPCK-C promotor transcriptional activity, and co-stimulation with AICAR blunted this forskolin-induced increase (*bars 1–4* of Fig. 5*B*). In wild-type GSK3β-overexpressing cells, although basal PEPCK-C transcriptional activity was increased as compared with that in LacZ-cells (*bars 1* and *5* of Fig. 5*B*), responses to forskolin and AICAR were quite similar (*bars 5–8* of Fig. 5*B*). However, in active mutant of GSK3β(S9G)-overexpressing cells, PEPCK-C promotor transcriptional activities under basal and AICAR-stimulated conditions were both significantly increased (*bars 9–12* of Fig. 5*B*), as compared with that in wild-type GSK3β-overexpressing cells. In addition, it should be noted that AICAR-induced suppression of PEPCK-C promotor transcriptional activity was observed in wild-type GSK3β-overexpressing cells, but this effect was nearly abolished in the GSK3β(S9G)-overexpressing cells (*bars 9* and *10* of Fig. 5*B*). Thus, it was revealed that expression of constitutively active GSK3β(S9G) enhanced PEPCK-C transcription in HepG2 cells, which suggests phosphorylation of Ser-9 of GSK3β is involved in the mechanism underlying AMPK or AICAR-induced PEPCK-C gene suppression.

AMPK Increases GSK3β(Ser-9) Phosphorylation but Decreases CREB Phosphorylation (Ser-129) in HepG2 Cells—To test whether activators of AMPK have a regulatory influence on GSK3β, HepG2 cells were treated with the AMPK activator AICAR, and phosphorylations of CREB and GSK3β were measured using immunoblot analyses with the corresponding phospho-specific antibodies. When cells were treated with 2 mM AICAR for 1 h, phosphorylation of GSK3β was significantly increased, whereas CREB phosphorylation was reduced (Fig. 6*A*). In contrast, when the cells were treated with the selective AMPK inhibitor Compound C, phosphorylation of GSK3β at Ser-9 was reduced, and that of CREB at Ser-129 was slightly

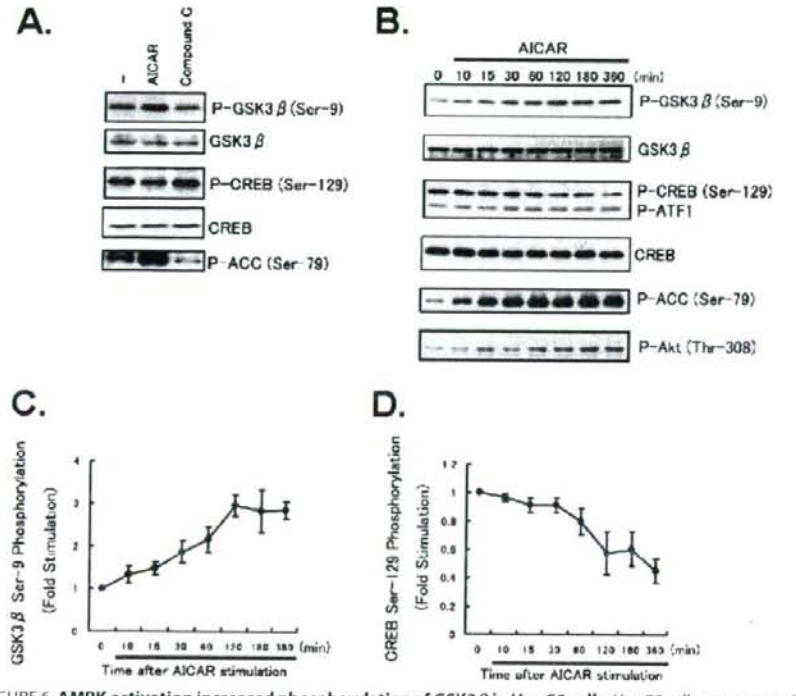

FIGURE 6. **AMPK activation increased phosphorylation of GSK3β in HepG2 cells.** HepG2 cells were treated with AICAR (2 mM) or the selective AMPK inhibitor Compound C (20 μM). *A*, immunoblot analyses were performed with HepG2 cell extracts prepared using anti-GSK3β, anti-phospho (*P-*)-GSK3β (Ser-9), anti-CREB, anti-phospho-CREB (Ser-129), or anti-phospho-ACC (Ser-79) antibody as indicated. *B*, Western blot analyses of time-dependent effects were performed with HepG2 cell extracts prepared using anti-GSK3β, anti-phospho-GSK3β (Ser-9), anti-CREB, anti-phospho-CREB (Ser-129), anti-phospho-Akt (Thr-308), or anti-phospho-ACC (Ser-79) antibody. *Panels C* and *D*, show the results of densitometric analysis of phospho-GSK3β (Ser-9) and phospho-CREB (Ser-129) as the mean ± S.E. of three samples.

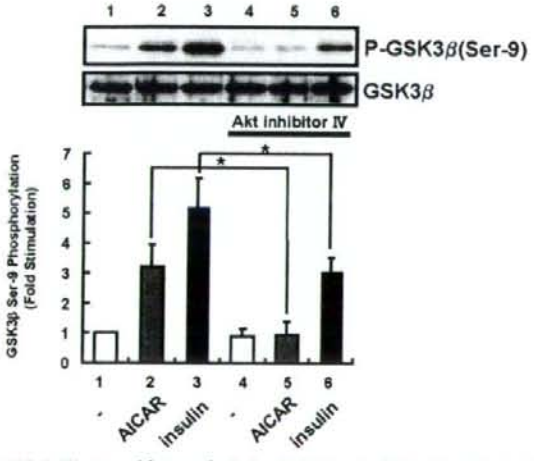

FIGURE 7. **Western blot analysis in AICAR-treated HepG2 cells in the absence or the presence of Akt inhibitor.** The Ser-9 phosphorylation (*P-*) levels of GSK3β were detected by Western blotting using an anti-P-Ser-9-Gsk3β antibody (*upper panel*). HepG2 cells were detected by treatment with AICAR (2 mM) for 1 h or insulin (1 μM) for 15 min after pretreatment with or without 10 μM Akt inhibitor IV. Pretreatment with 10 μM Akt inhibitor IV inhibited AICAR-induced GSK3β phosphorylation (*P*). The *lower panel* shows the results of densitometric analysis of phospho-GSK3β (Ser-9) as the mean ± S.E. of three samples. *, $p < 0.05$.

increased (Fig. 6*A*). Thus, AMPK activation caused phosphorylation of GSK3β via a mechanism that was blocked by the AMPK inhibitor Compound C, indicating that an AMPK-dependent effect contributes to this response to AICAR. *Panel B* of Fig. 6 shows the time-courses of AICAR-induced phosphorylation of GSK3β at Ser-9, CREB phosphorylation at Ser-129, ACC phosphorylation at Ser-79, and Akt phosphorylation at Thr-308. The time-courses of decreased CREB phosphorylation (Ser-129) and increased GSK3β phosphorylation were very similar (*panels C* and *D* of Fig. 6). These actions were evident within 10 min of treatment and were maintained for 360 min. Phosphorylation of Ser-133 was unchanged by AICAR stimulation in HepG2 cells (data not shown). The data suggest GSK3β integrate AMPK signaling pathways to promote CREB Ser-129 phosphorylation. We also did these experiments in primary hepatocytes (supplemental Fig. 1). With only AICAR treatment, *i.e.* no activation of AMPK, there was neither phosphorylation of GSK3β nor dephosphorylation of CREB. However, in the presence of dibutyryl-cAMP, AICAR treatment induced phosphorylation of Ser-9-GSK3β and reduced that of Ser-129-CREB. These results demonstrate that AICAR triggers phosphorylation of GSK3β in the presence of dibutyryl-cAMP-increased protein kinase A activation and suggest that AICAR regulates the phosphorylations of GSK3β in parallel with its effects on gluconeogenesis.

Phosphatidylinositol 3-Kinase/Akt Pathway Is Necessary for AMPK-induced GSK3β Phosphorylation—To examine whether phosphatidylinositol 3-kinase and Akt activations are necessary for AMPK-mediated GSK3β phosphorylation, HepG2 cells were stimulated with AICAR with or without pretreatment with 10 μM Akt inhibitor IV ((Fig. 7). Both insulin-induced and AICAR-induced GSK3β phosphorylations were inhibited by preincubation with Akt inhibitor IV. Akt phosphorylation on Thr-308 was increased in a time-dependent manner (Fig. 6*B*). Thus, AMPK-induced GSK3β phosphorylation is likely to be mediated by the Akt pathway.

AICAR Suppresses CREB-CBP Interactions—Protein kinase A reportedly phosphorylates CREB at Ser-133, and phosphorylation of CREB increases its affinity for CREs. Ser-129, a consensus GSK3β phospho-accepter site, has been proposed to regulate CREB activity in conjunction with Ser-133 after cAMP induction. Because the CREB transcriptional coactivator, CREB-binding protein (CBP/P300), is a nuclear protein that

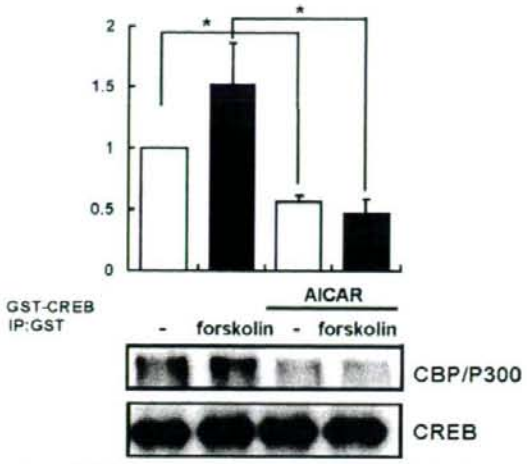

FIGURE 8. **AICAR stimulation inhibited CREB-CBP/P300 interaction.** Amounts of CBP associated with CREB were determined by immunoprecipitation with extracts obtained from transfected HepG2 cells. HepG2 cells transfected with GST-tagged CREB were serum-starved overnight before incubation with AICAR (2 mM) with or without 10 μM forskolin for 1 h. HepG2 cells transfected with GST-tagged CREB were extracted and subjected to immunoprecipitation using GST-specific antibody. Shown is a Western blot of GST-tagged CREB-transfected HepG2 cell lysates with a CBP/P300-specific antibody showing immunoprecipitation of exogenously expressed GST-tagged CREB with endogenous CBP/P300 (*upper lanes*, immunoprecipitation of endogenous CBP/P300 from GST-tagged CREB transfected cells with the CBP/P300-specific antibody; *lower lane*, immunoprecipitation (*IP*) of GST-tagged CREB with the anti-CREB antibody). The results are presented as the mean ± S.E. of three independent experiments.

binds specifically to the protein kinase A-phosphorylated form of CREB and can activate transcription (33), we examined how the forskolin-promoted CREB-CBP interaction was regulated via AICAR stimulation.

Forskolin treatment increased the interaction between endogenous CBP/P300 and transfected GST-CREB in HepG2 cells as previously reported (Fig. 8). It was revealed that AICAR treatment markedly decreased this interaction (Fig. 8). This result suggested that the affinity of CREB for CBP/P300 was negatively regulated by suppression of CREB Ser-129 phosphorylation in response to AICAR stimulation.

DISCUSSION

Hepatic gluconeogenesis is strictly regulated to maintain whole-body glucose homeostasis, and several hormones such as insulin and glucagons are involved in this regulation. PEPCK-C has been regarded as the key enzyme determining the rate of hepatic gluconeogenesis, but recent studies on PEPCK-C gene knock-out mice suggest that PEPCK-C functions as an integrator of hepatic energy metabolism, including those of lipid and glycogen (34–36). The promoter region of the PEPCK-C gene contains the CRE domain, which was shown to play an important role in PEPCK-C gene expression (30, 31, 37–39). Glucagon and forskolin, via increased cAMP, reportedly increase PEPCK-C gene expression by stimulating protein kinase A-mediated phosphorylation of CREB at Ser-133 (40–43). Recently, the coactivator of CREB termed TORC2 was reported to be important for the regulation of CRE transcriptional activity and PEPCK-C gene expression (12). TORC2 is reportedly phosphorylated by AMPK and SIK, and phosphorylated TORC2 binds to 14-3-3 protein and is thereby removed from the nucleus to the cytoplasm (16). Depletion of nuclear TORC2 led to the suppression of CRE transcriptional activity (44). Thus, AMPK-induced PEPCK-C gene suppression is likely to be mediated by TORC2 phosphorylation. However, in this study we demonstrated another mechanism to underlie AMPK-induced PEPCK-C gene suppression. This novel mechanism involves GSK3β phosphorylation and subsequent CREB dephosphorylation.

We demonstrated for the first time that AMPK activation increases GSK3β phosphorylation in not only cultured cells such as HepG2 but also in the mouse liver. This phosphorylation in the liver was rapidly induced (within 15 min of AICAR stimulation) and persisted for at least 2 h, indicating physiological significance. In addition, suppression of AMPK with the selective inhibitor Compound C blocked GSK3β phosphorylation induced by AICAR. Because the Akt inhibitor attenuated AICAR-induced GSK3β phosphorylation, it seems unlikely that AMPK directly phosphorylates GSK3β. Indeed, AICAR stimulation does not activate phosphatidylinositol 3-kinase (data not shown) but does increase Akt phosphorylation. Thus, although the exact molecular mechanism cannot be identified from our data, several possibilities can be considered. For example, AMPK activation may affect the activity of PDK1 or the mTOR-Rictor complex (45, 46). Another possibility is that the dephosphorylation of Akt or GSK3β is suppressed by AMPK activation. Indeed, a recent study also found Akt to be dephosphorylated after AICAR treatment in differentiated hippocampal neurons (47). Alternatively, inhibition of other kinases might be involved in the effects of AICAR because it was recently reported that AICAR inhibits the Ser-9 phosphorylation of GSK3β induced by co-treatment with a phorbol ester activator of protein kinase C plus the calcium ionophore ionomycin. Further studies are necessary to clarify this issue.

Phosphorylation of GSK3 at an NH_2-terminal serine residue (Ser-21 and Ser-9 in GSK-3α and -3β, respectively) renders it inactive. Administration of specific inhibitors of GSK3β such as L803-mts reportedly not only increases hepatic glycogen synthesis but also decreases glucose production with decreased levels of PEPCK-C mRNA in fa/fa rats (48) and ob/ob mice (49). However, the molecular events underlying the regulation of PEPCK-C gene expression by GSK3β remain unclear. Because a previous study showed that GSK3β phosphorylates CREB at Ser-129 (20), we considered the possibility that GSK3β phosphorylation contributes to AMPK-induced PEPCK-C gene suppression. AICAR stimulation induced GSK3β phosphorylation and CREB dephosphorylation in HepG2 cells with very similar time-courses (Fig. 6). In addition, AMPK stimulation reduced PEPCK-C promoter activity in HepG2 cells, and the GSK3β inhibitor SB-415286 and AICAR both strongly suppressed CRE activity. Importantly, AICAR-induced suppression of PEPCK-C promoter activity was significantly attenuated by overexpressing the constitutively active mutant of GSK3β(S9G). These findings strongly suggest that inactivation of GSK3β is necessary for AMPK-induced PEPCK-C promoter and CRE activity suppressions. We also performed reporter assays using Gal4-CREB and Gal4-TORC2 reporter systems.

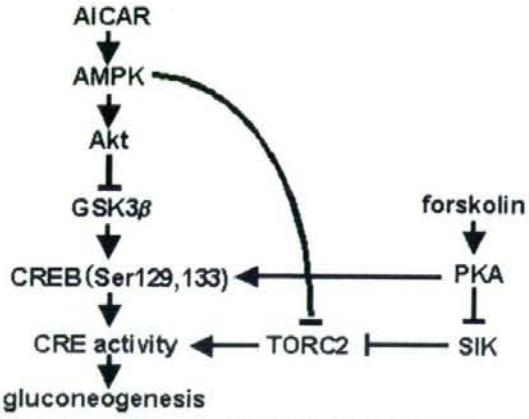

FIGURE 9. **A model of the role of the AMPK-GSK3β-CREB signaling pathway in gluconeogenesis.** *PKA*, protein kinase A.

SB-415286 suppressed CREB reporter activities while only slightly affecting those of TORC2 (Fig. 3, *A* and *B*). Stimulation of hepatocytes with SB415286 did not shift the mobility of TORC2 according to the presence or absence of forskolin (Fig. 4*A*). These results showed GSK3β inactivation to directly inhibit CREB.

The importance of Ser-133 phosphorylation in stimulating CREB activity has been recognized (50, 51). Phosphorylation of CREB at Ser-133 also creates a consensus site for phosphorylation by GSK3β at Ser-129 (21). Substitution of Ser-129 by Ala strongly impaired forskolin-induced CREB-dependent transcription in PC12 cells (21). We observed the suppression of Ser-129 phosphorylation by AICAR stimulation to decrease CREB-CBP interactions. These results showed double-phosphorylated CREB (Ser-129 and -133) to promote the TORC2-CBP interaction. GSK3β may also play a physiological role in cAMP signaling, as cAMP-induced stimulation of CREB activity depended on the phosphorylation of Ser-129 (Fig. 9).

Taken together, our findings indicate that pathways activated in parallel by this agent then concomitantly activate AMPK and phosphorylate Akt and, consequently, GSK3β. These results indicate that actions ascribed to AMPK after AICAR treatment may be influenced by the concomitant modulatory actions of this drug on Akt and GSK3β. AMPK and Akt generally have opposing roles in cellular metabolism. AMPK is activated when AMP levels increase in conjunction with decreased ATP levels, and activated AMPK inhibits anabolic processes and promotes catabolism to minimize ATP utilization while promoting ATP production. On the other hand, Akt generally promotes anabolic cellular functions that utilize ATP, such as proliferation and cell growth, although Akt may share with AMPK the ability to promote ATP synthesis by different mechanisms. Thus, the combined effects of AICAR on AMPK and Akt may enhance the outcomes that have been ascribed to their activating effects on AMPK.

In conclusion, AMPK activation increases GSK3β phosphorylation *in vivo*. Reduced CREB phosphorylation (Ser-129) associated with inactivation of GSK3β by Ser-9 phosphorylation may be the major mechanism underlying PEPCK-C gene suppression by AMPK-activating agents such as biguanide, leptin, and adiponectin. Thus, it is very likely that two mechanisms independently mediate the AMPK-induced suppression of PEPCK-C expression. We agree that TORC2 phosphorylation by AMPK is important, but the GSK3β-mediated pathway plays an additional, possibly critical, role in PEPCK-C gene suppression.

REFERENCES

1. Vincent, M. F., Erion, M. D., Gruber, H. E., and Van den Berghe, G. (1996) *Diabetologia* **39,** 1148–1155
2. Stapleton, D., Mitchelhill, K. I., Gao, G., Widmer, J., Michell, B. J., Teh, T., House, C. M., Fernandez, C. S., Cox, T., Witters, L. A., and Kemp, B. E. (1996) *J. Biol. Chem.* **271,** 611–614
3. Winder, W. W., and Hardie, D. G. (1999) *Am. J. Physiol.* **277,** E1–E10
4. Zhou, G., Myers, R., Li, Y., Chen, Y., Shen, X., Fenyk-Melody, J., Wu, M., Ventre, J., Doebber, T., Fujii, N., Musi, N., Hirshman, M. F., Goodyear, L. J., and Moller, D. E. (2001) *J. Clin. Investig.* **108,** 1167–1174
5. Yamauchi, T., Kamon, J., Minokoshi, Y., Ito, Y., Waki, H., Uchida, S., Yamashita, S., Noda, M., Kita, S., Ueki, K., Eto, K., Akanuma, Y., Froguel, P., Foufelle, F., Ferre, P., Carling, D., Kimura, S., Nagai, R., Kahn, B. B., and Kadowaki, T. (2002) *Nat. Med.* **8,** 1288–1295
6. Lochhead, P. A., Salt, I. P., Walker, K. S., Hardie, D. G., and Sutherland, C. (2000) *Diabetes* **49,** 896–903
7. Cool, B., Zinker, B., Chiou, W., Kifle, L., Cao, N., Perham, M., Dickinson, R., Adler, A., Gagne, G., Iyengar, R., Zhao, G., Marsh, K., Kym, P., Jung, P., Camp, H. S., and Frevert, E. (2006) *Cell Metab.* **3,** 403–416
8. Towler, M. C., and Hardie, D. G. (2007) *Circ. Res.* **100,** 328–341
9. Bady, I., Marty, N., Dallaporta, M., Emery, M., Gyger, J., Tarussio, D., Foretz, M., and Thorens, B. (2006) *Diabetes* **55,** 988–995
10. Winder, W. W., Wilson, H. A., Hardie, D. G., Rasmussen, B. B., Hutber, C. A., Call, G. B., Clayton, R. D., Conley, L. M., Yoon, S., and Zhou, B. (1997) *J. Appl. Physiol.* **82,** 219–225
11. Munday, M. R., Campbell, D. G., Carling, D., and Hardie, D. G. (1988) *Eur. J. Biochem.* **175,** 331–338
12. Koo, S. H., Flechner, L., Qi, L., Zhang, X., Screaton, R. A., Jeffries, S., Hedrick, S., Xu, W., Boussouar, F., Brindle, P., Takemori, H., and Montminy, M. (2005) *Nature* **437,** 1109–1111
13. Conkright, M. D., Canettieri, G., Screaton, R., Guzman, E., Miraglia, L., Hogenesch, J. B., and Montminy, M. (2003) *Mol. Cell* **12,** 413–423
14. Iourgenko, V., Zhang, W., Mickanin, C., Daly, I., Jiang, C., Hexham, J. M., Orth, A. P., Miraglia, L., Meltzer, J., Garza, D., Chirn, G. W., McWhinnie, E., Cohen, D., Skelton, J., Terry, R., Yu, Y., Bodian, D., Buxton, F. P., Zhu, J., Song, C., and Labow, M. A. (2003) *Proc. Natl. Acad. Sci. U. S. A.* **100,** 12147–12152
15. Shaw, R. J., Lamia, K. A., Vasquez, D., Koo, S. H., Bardeesy, N., Depinho, R. A., Montminy, M., and Cantley, L. C. (2005) *Science* **310,** 1642–1646
16. Screaton, R. A., Conkright, M. D., Katoh, Y., Best, J. L., Canettieri, G., Jeffries, S., Guzman, E., Niessen, S., Yates, J. R., III, Takemori, H., Okamoto, M., and Montminy, M. (2004) *Cell* **119,** 61–74
17. Bittinger, M. A., McWhinnie, E., Meltzer, J., Iourgenko, V., Latario, B., Liu, X., Chen, C. H., Song, C., Garza, D., and Labow, M. (2004) *Curr. Biol.* **14,** 2156–2161
18. Zhou, X. Y., Shibusawa, N., Naik, K., Porras, D., Temple, K., Ou, H., Kaihara, K., Roe, M. W., Brady, M. J., and Wondisford, F. E. (2004) *Nat. Med.* **10,** 633–637
19. Chrivia, J. C., Kwok, R. P., Lamb, N., Hagiwara, M., Montminy, M. R., and Goodman, R. H. (1993) *Nature* **365,** 855–859
20. Fiol, C. J., Williams, J. S., Chou, C. H., Wang, Q. M., Roach, P. J., and Andrisani, O. M. (1994) *J. Biol. Chem.* **269,** 32187–32193
21. Tyson, D. R., Swarthout, J. T., Jefcoat, S. C., and Partridge, N. C. (2002) *Endocrinology* **143,** 674–682
22. Tullai, J. W., Chen, J., Schaffer, M. E., Kamenetsky, E., Kasif, S., and Cooper, G. M. (2007) *J. Biol. Chem.* **282,** 9482–9491
23. Yeagley, D., Agati, J. M., and Quinn, P. G. (1998) *J. Biol. Chem.* **273,** 18743–18750
24. Lipina, C., Huang, X., Finlay, D., McManus, E. J., Alessi, D. R., and Suth-

erland, C. (2005) *Biochem. J.* **392,** 633–639
25. Ogihara, T., Shin, B. C., Anai, M., Katagiri, H., Inukai, K., Funaki, M., Fukushima, Y., Ishihara, H., Takata, K., Kikuchi, M., Yazaki, Y., Oka, Y., and Asano, T. (1997) *J. Biol. Chem.* **272,** 12868–12873
26. Doi, J., Takemori, H., Lin, X. Z., Horike, N., Katoh, Y., and Okamoto, M. (2002) *J. Biol. Chem.* **277,** 15629–15637
27. Sakoda, H., Gotoh, Y., Katagiri, H., Kurokawa, M., Ono, H., Onishi, Y., Anai, M., Ogihara, T., Fujishiro, M., Fukushima, Y., Abe, M., Shojima, N., Kikuchi, M., Oka, Y., Hirai, H., and Asano, T. (2003) *J. Biol. Chem.* **278,** 25802–25807
28. Lochhead, P. A., Coghlan, M., Rice, S. Q., and Sutherland, C. (2001) *Diabetes* **50,** 937–946
29. Sasaki, K., Cripe, T. P., Koch, S. R., Andreone, T. L., Petersen, D. D., Beale, E. G., and Granner, D. K. (1984) *J. Biol. Chem.* **259,** 15242–15251
30. Short, J. M., Wynshaw-Boris, A., Short, H. P., and Hanson, R. W. (1986) *J. Biol. Chem.* **261,** 9721–9726
31. Hanson, R. W., and Reshef, L. (1997) *Annu. Rev. Biochem.* **66,** 581–611
32. Croniger, C., Leahy, P., Reshef, L., and Hanson, R. W. (1998) *J. Biol. Chem.* **273,** 31629–31632
33. Vo, N., and Goodman, R. H. (2001) *J. Biol. Chem.* **276,** 13505–13508
34. She, P., Shiota, M., Shelton, K. D., Chalkley, R., Postic, C., and Magnuson, M. A. (2000) *Mol. Cell. Biol.* **20,** 6508–6517
35. She, P., Burgess, S. C., Shiota, M., Flakoll, P., Donahue, E. P., Malloy, C. R., Sherry, A. D., and Magnuson, M. A. (2003) *Diabetes* **52,** 1649–1654
36. Hakimi, P., Johnson, M. T., Yang, J., Lepage, D. F., Conlon, R. A., Kalhan, S. C., Reshef, L., Tilghman, S. M., and Hanson, R. W. (2005) *Nutr. Metab.* **2,** 33–44
37. Foretz, M., Ancellin, N., Andreelli, F., Saintillan, Y., Grondin, P., Kahn, A., Thorens, B., Vaulont, S., and Viollet, B. (2005) *Diabetes* **54,** 1331–1339
38. Roesler, W. J., Vandenbark, G. R., and Hanson, R. W. (1989) *J. Biol. Chem.* **264,** 9657–9664
39. Klemm, D. J., Roesler, W. J., Liu, J. S., Park, E. A., and Hanson, R. W. (1990) *Mol. Cell. Biol.* **10,** 480–485
40. Leahy, P., Crawford, D. R., Grossman, G., Gronostajski, R. M., and Hanson, R. W. (1999) *J. Biol. Chem.* **274,** 8813–8822
41. Herzig, S., Long, F., Jhala, U. S., Hedrick, S., Quinn, R., Bauer, A., Rudolph, D., Schutz, G., Yoon, C., Puigserver, P., Spiegelman, B., and Montminy, M. (2001) *Nature* **413,** 179–183
42. Parker, D., Ferreri, K., Nakajima, T., LaMorte, V. J., Evans, R., Koerber, S. C., Hoeger, C., and Montminy, M. R. (1996) *Mol. Cell. Biol.* **16,** 694–703
43. Sassone-Corsi, P. (1998) *Int. J. Biochem. Cell Biol.* **30,** 27–38
44. Boer, U., Eglins, J., Krause, D., Schnell, S., Schofl, C., and Knepel, W. (2007) *Biochem. J.* **408,** 69–77
45. Sarbassov, D. D., Guertin, D. A., Ali, S. M., and Sabatini, D. M. (2005) *Science* **307,** 1098–1101
46. Tzatsos, A., and Kandror, K. V. (2006) *Mol. Cell. Biol.* **26,** 63–76
47. King, T. D., Song, L., and Jope, R. S. (2006) *Biochem. Pharmacol.* **71,** 1637–1647
48. Cline, G. W., Johnson, K., Regittnig, W., Perret, P., Tozzo, E., Xiao, L., Damico, C., and Shulman, G. I. (2002) *Diabetes* **51,** 2903–2910
49. Kaidanovich-Beilin, O., and Eldar-Finkelman, H. (2006) *J. Pharmacol. Exp. Ther.* **316,** 17–24
50. Sands, W. A., and Palmer, T. M. (2008) *Cell. Signal.* **20,** 460–466
51. Johannessen, M., and Moens, U. (2007) *Front. Biosci.* **12,** 1814–1832

Activation of hypothalamic S6 kinase mediates diet-induced hepatic insulin resistance in rats

Hiraku Ono,[1] Alessandro Pocai,[1] Yuhua Wang,[1] Hideyuki Sakoda,[2] Tomoichiro Asano,[3] Jonathan M. Backer,[1] Gary J. Schwartz,[1] and Luciano Rossetti[1]

[1]Department of Medicine, Diabetes Research Center, Albert Einstein College of Medicine, New York, New York, USA. [2]Department of Internal Medicine, Graduate School of Medicine, University of Tokyo, Tokyo, Japan. [3]Graduate School of Biomedical Sciences, Hiroshima University, Hiroshima, Japan.

Prolonged activation of p70 S6 kinase (S6K) by insulin and nutrients leads to inhibition of insulin signaling via negative feedback input to the signaling factor IRS-1. Systemic deletion of S6K protects against diet-induced obesity and enhances insulin sensitivity in mice. Herein, we present evidence suggesting that hypothalamic S6K activation is involved in the pathogenesis of diet-induced hepatic insulin resistance. Extending previous findings that insulin suppresses hepatic glucose production (HGP) partly via its effect in the hypothalamus, we report that this effect was blunted by short-term high-fat diet (HFD) feeding, with concomitant suppression of insulin signaling and activation of S6K in the mediobasal hypothalamus (MBH). Constitutive activation of S6K in the MBH mimicked the effect of the HFD in normal chow–fed animals, while suppression of S6K by overexpression of dominant-negative S6K or dominant-negative raptor in the MBH restored the ability of MBH insulin to suppress HGP after HFD feeding. These results suggest that activation of hypothalamic S6K contributes to hepatic insulin resistance in response to short-term nutrient excess.

Introduction

Insulin resistance plays an important role in the pathogenesis of type 2 diabetes. It is well established that excess nutrient intake and chronic hyperinsulinemia cause insulin resistance. The mammalian target of rapamycin/S6 kinase (mTOR/S6K) pathway has emerged as a promising molecular mediator of insulin resistance because it is activated by both insulin and nutrients (1–3). Insulin signaling is characterized by activation of the insulin receptor, followed by tyrosine phosphorylation of IRS proteins, PI3K activation, and Akt phosphorylation. Akt then inhibits tuberous sclerosis complex 1/2 by phosphorylation, resulting in Rheb activation, and activated Rheb then binds to and activates mTOR (4). How nutrients drive the mTOR/S6K pathway is less well understood, although AMPK (5), VPS34 (6, 7), and MAP4K3 (8) have been suggested as candidate mediators. Thus, mTOR sits at a critical juncture between insulin and nutrient signaling, making it important both for insulin signaling downstream from Akt and for nutrient sensing. It is also possible that activation of mTOR by nutrient signaling may, at least in part, offset its effects as a distal mediator of insulin action. The mTOR/S6K pathway is not only downstream from insulin signaling, but also upstream from it as a negative regulator, because S6K and/or mTOR phosphorylates several serine residues of IRS-1 to inhibit insulin signaling at the level of IRS-1 (9–12). Through this negative feedback mechanism, bidirectional changes in nutrient availability may lead to adaptive modifications in insulin signaling. In strong support of the physiological relevance of this mechanism, mice carrying a systemic deletion of S6K are lean and display enhanced insulin sensitivity (13). However, the critical sites involved in S6K mediation of insulin sensitivity have yet to be identified.

Hypothalamic insulin signaling reportedly contributes to the regulation of hepatic glucose production (HGP) in rodents (14–18). This indirect effect of insulin on the liver may play a major role in determining insulin-mediated suppression of HGP by suppressing hepatic gluconeogenesis in these species. Furthermore, short-term increases in nutrient intake selectively blunt insulin's action on HGP. In hyperinsulinemic-euglycemic clamp studies in rats, we and others have shown that 3 d of high-fat diet (HFD) feeding is sufficient to induce hepatic insulin resistance, while the induction of peripheral insulin resistance requires more chronic nutrient excess (19, 20). Taken together, these data suggest that hepatic insulin resistance induced by both nutrient excess and hyperinsulinemia could stem from blunted hypothalamic insulin signaling. In this study, we investigated whether the ability of intrahypothalamic insulin — administered via the mediobasal hypothalamus (MBH) — to suppress HGP is affected by short-term HFD feeding, and we demonstrated the involvement of the hypothalamic mTOR/S6K pathway in diet-induced hepatic insulin resistance. We found that S6K activity increased during short-term HFD feeding and that adenoviral overactivation and suppression of hypothalamic S6K respectively mimicked and blocked the inhibitory effects of HFD feeding on central insulin-induced suppression of HGP.

Results

Short-term HFD feeding induces hypothalamic insulin resistance. Previous hyperinsulinemic-euglycemic clamp studies demonstrated that HFD feeding of rats induces hepatic insulin resistance in just 3 d (19, 20), while HFD feeding for 1–3 wk is required for insulin resistance to emerge in muscle and adipose tissue. Taken together with the fact that hypothalamic insulin is involved in the regulation of HGP, these findings suggest the possibility that hypothalamic

Nonstandard abbreviations used: CA-S6K, constitutively active S6K; DN-S6K, dominant-negative S6K; HFD, high-fat diet; HGP, hepatic glucose production; MBH, mediobasal hypothalamus; mTOR, mammalian target of rapamycin; NC, normal chow; PTP-1B, protein tyrosine phosphatase–1B; Raptor/ΔCT, C terminal–truncated Raptor; S6K, S6 kinase; TORC1, target of rapamycin complex 1.

Conflict of interest: The authors have declared that no conflict of interest exists.

Citation for this article: *J. Clin. Invest.* **118**:2959–2968 (2008). doi:10.1172/JCI34777

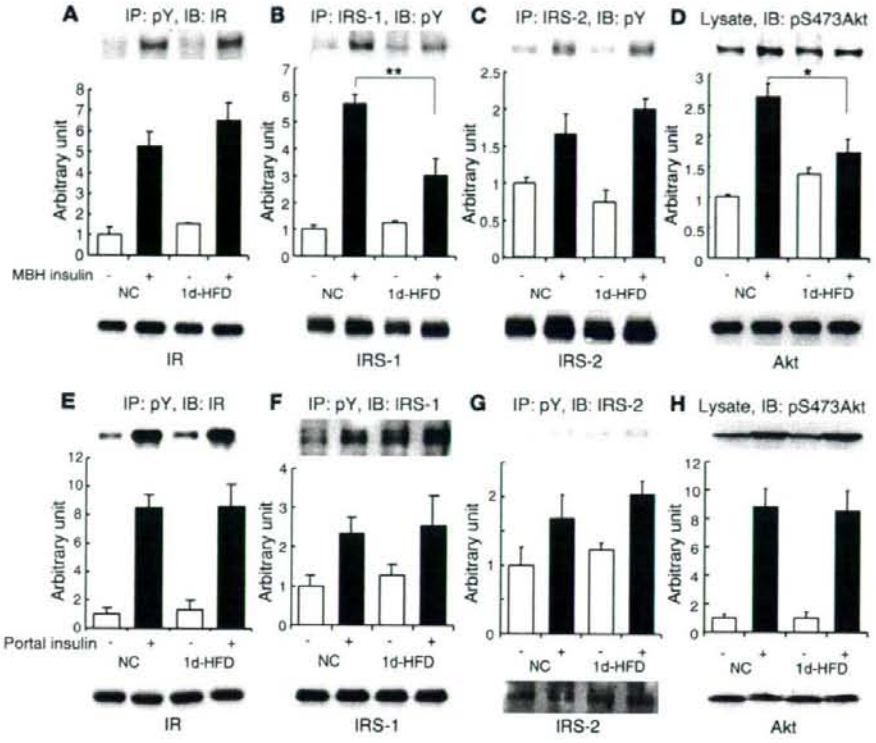

Figure 1

HFD feeding for 1 d blunts insulin signaling in the MBH at the level of IRS-1 without altering hepatic insulin signaling. Rats were fed NC or HFD for 1 d. Insulin was infused into the MBH (4 μU) or the portal vein (1 U/kg), and 15 min or 3 min later, respectively, MBH (**A–D**) or the liver (**E–H**) was harvested and analyzed. Tyrosine phosphorylations of IR (**A** and **E**), IRS-1 (**B** and **F**), and IRS-2 (**C** and **G**) were studied by immunoprecipitation with anti-phosphotyrosine (pY) antibody and blotted with anti-IR (**A** and **E**), anti–IRS-1 (**F**), anti–IRS-2 (**G**), or immunoprecipitation with anti–IRS-1 (**B**) or anti–IRS-2 (**C**) antibodies and blotting with anti-phosphotyrosine antibody. (**D** and **H**) Tissue lysates were blotted with anti-pSer473 Akt antibody. Graphs show the ratio of phosphoproteins to total proteins. $^{*}P < 0.05$; $^{**}P < 0.01$.

insulin resistance is relatively rapidly induced by HFD feeding and that this hypothalamic effect could promote hepatic insulin resistance. To investigate the putative early molecular and physiological mechanisms mediating HFD-induced insulin resistance, we examined hypothalamic insulin signaling 1 d after a marked increase in nutrient intake. We infused 4 μU insulin into the MBH of rats over a 5-min period and assessed insulin signaling in the MBH 15 min after this infusion. The ability of insulin to stimulate IRS-1 tyrosine phosphorylation (Figure 1B) and Akt serine phosphorylation at Ser473 (Figure 1D) was severely impaired after 1 d of HFD feeding, while tyrosine phosphorylation of the IR (Figure 1A) and IRS-2 (Figure 1C) was not affected.

We also investigated whether insulin signaling in the liver is affected in this model. At 3 min after portal vein injection of 1 U/kg insulin, tyrosine phosphorylation of IR (Figure 1E), IRS-1 (Figure 1F), and IRS-2 (Figure 1G) as well as serine phosphorylation of Akt (Figure 1H) in rats fed HFD for 1 d did not differ significantly from those seen with normal chow (NC) feeding.

Using a protocol with which we previously showed the ability of central insulin (17), glucose (21), and fatty acids (22) to suppress HGP (Figure 2A), we then performed a pancreatic insulin clamp study to investigate whether the ability of central insulin to suppress glucose production is affected in short-term HFD-fed rats. Glucose production was determined both in absolute values (Figure 2C) and as the percent ratio of basal to clamped levels (Figure 2D). In rats fed NC, MBH insulin significantly increased the glucose infusion required to maintain euglycemia during the clamp (Figure 2B) and decreased HGP by 28% (Figure 2, C and D) compared with vehicle, as previously reported (18). While MBH insulin significantly suppressed glucose production in animals maintained on NC, 1-d HFD feeding completely blocked this effect, consistent with the blunted hypothalamic insulin signaling shown in Figure 1. The hypothalamic effects of insulin on glucose requirements (Figure 2B) and on HGP (Figure 2, C and D) were blunted in HFD-fed rats. Peripheral glucose uptake was slightly increased in 1-d HFD-fed rats with MBH insulin infusion compared with NC-fed rats with vehicle infusion (Figure 2E).

To investigate the potential mechanisms responsible for the rapid impairment of hypothalamic insulin signaling, we measured S6K activity, protein tyrosine phosphatase-1B (PTP-1B) protein amount, and the level and phosphorylation of JNK protein in the MBH. S6K activity increased approximately 45% in MBH of

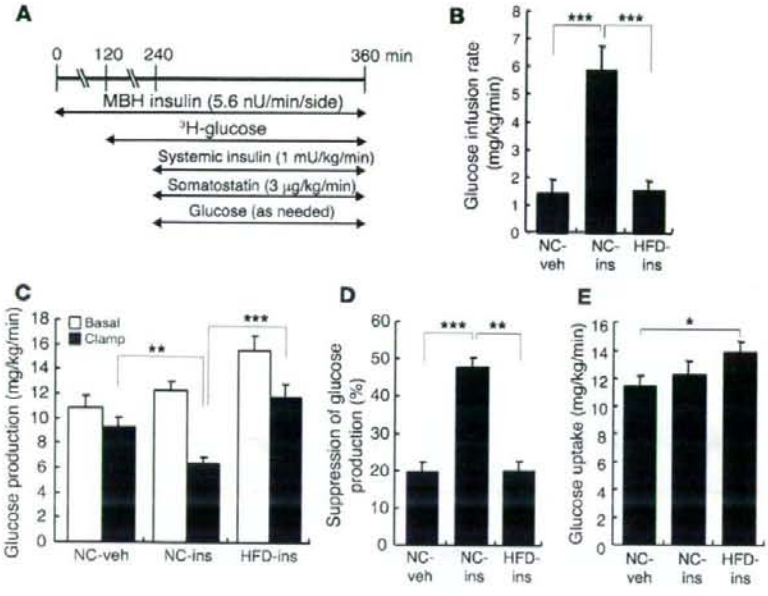

Figure 2
HFD feeding for 1 d induces insulin resistance in the brain-liver circuit. Rats were fed NC or HFD (171% of the energy of NC) for 1 d. After 5 h of fasting, vehicle (veh) or 4 μU insulin (ins) was infused into the MBH for the entire 6-h duration of the clamp study. (**A**) Clamp protocol. Equilibration period, 0–120 min; basal period, 120–240 min; insulin clamp period, 240–360 min, during which systemic insulin and glucose were continuously infused and the rate of the latter was adjusted to maintain euglycemia. (**B**) Glucose infusion rate required to maintain euglycemia during the clamp period. (**C**) HGP during the basal and clamp periods. (**D**) Clamp/basal HGP suppression ratio. (**E**) Peripheral glucose uptake during the clamp period. $^{*}P < 0.05$; $^{**}P < 0.01$; $^{***}P < 0.001$.

HFD-fed rats (Figure 3A), while the level and phosphorylation of JNK protein and expression of PTP-1B were unaffected (data not shown). As shown in Figure 3B, the increase in MBH S6K activity with HFD feeding was comparable to that induced by MBH insulin. In addition, raising insulin concentrations 10-fold did not result in greater S6K activation, which suggests that this level of S6K activity is maximal in the MBH. We also investigated the time course of activation. S6K activity reached maximal levels following the first day of HFD feeding (Figure 3C), indicating that this phenomenon occurs early during HFD feeding. This maximal level was maintained for at least 7 d of HFD feeding, demonstrating HFD-induced persistence of MBH S6K activation.

Overactivation of S6K in the hypothalamus blunts the ability of insulin to suppress glucose production. Based on these results, we hypothesized that HFD-induced hepatic insulin resistance may be mediated by hypothalamic activation of S6K. Consequently, we injected an adenoviral vector encoding rat constitutively active S6K (CA-S6K; Figure 4A) or a LacZ control into the rat MBH. S6K is known to have 2 inhibitory regulatory domains in the N and the C terminus. The CA-S6K carries mutations in both N- and C-terminal regulatory domains that render the kinase rapamycin insensitive, and hence constitutively active. The constitutive activity of this construct has already been demonstrated by transfection in cultured cells (23, 24). We performed a functional validation of our virus in the hypothalamic GT1-7 cell line. As shown in Figure 4B, adenoviral overexpression of this construct markedly induced serine phosphorylation of all 3 known substrates of S6K1 (IRS-1, S6 ribosomal protein, and eIF4B), consistent with results previously obtained using other cell lines (23, 24). Figure 4C shows transgene overexpression levels in the MBH, as detected by immunoblotting with anti-Flag and anti-S6K antibodies. Overexpression of CA-S6K in the MBH was associated with a 4.5-fold increase in S6K activ-

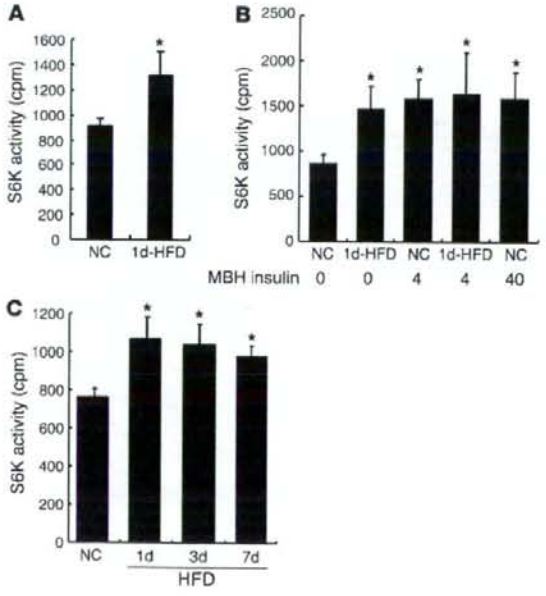

Figure 3
MBH S6K activity increased in the HFD-fed model. (**A**) S6K activity was assayed in the MBH of rats fed NC or HFD for 1 d. (**B**) At 12 d after MBH cannulation, rats fed NC or HFD for 1 d were fasted for 5 h and injected with 0, 4, or 40 μU insulin for 5 min. After 40 min, the MBH was harvested and processed for S6K assay. (**C**) Rats were fed HFD for 0, 1, 3, or 7 d. On the last day, all rats were fed 20 g NC or HFD. After 5 h of fasting, the MBH was harvested and processed for S6K assay. $^{*}P < 0.05$ versus NC.

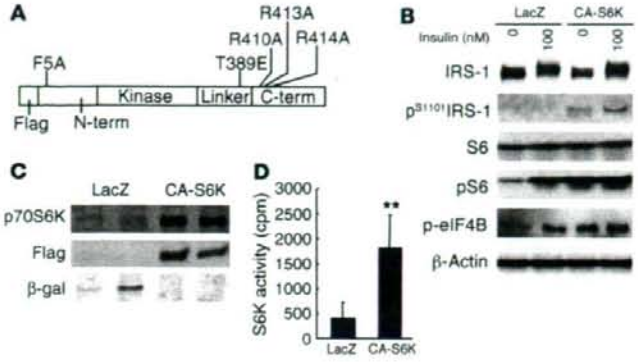

Figure 4
Hypothalamic overexpression of CA-S6K and functional validation in GT1-7 hypothalamic cells. (**A**) Construction of CA-S6K. (**B**) Adenovirus-infected GT1-7 cells were stimulated with insulin for 30 min. Serine phosphorylations in the basal state (0 nM insulin) of S6, IRS-1, and eIF4B were increased to maximal levels (comparable to LacZ expression with 100 nM insulin) by CA-S6K overexpression ($P < 0.01$; $n = 2$). The ratios of phosphoproteins to total proteins, and of phosphoproteins to actin, were statistically analyzed. Representative bands are shown. (**C**) Expression of CA-S6K in the MBH. MBH tissue lysates obtained 12 d after viral injection were immunoblotted with anti-S6K, anti-M5-Flag, or anti–β-gal antibodies. (**D**) S6K activity in MBH samples. $^{**}P < 0.01$ versus LacZ.

ity in the MBH samples (Figure 4D), thereby exceeding the level we observed with HFD feeding or insulin stimulation (Figure 3B). We compared transgene expression levels in micropunch samples from the arcuate nucleus, paraventricular nucleus, and lateral hypothalamus using both S6K antibody and Flag-tagged antibody and confirmed that transgene overexpression was limited to the arcuate nucleus (Supplemental Figure 1).

We then examined the effects of the same dose of CA-S6K or control LacZ adenovirus in pancreatic clamp studies performed 12 d after the viral MBH injections (Figure 5A). Adenoviral expression of LacZ did not affect the ability of insulin to suppress HGP compared with animals without viral treatment (Figure 5, B–E). In contrast, CA-S6K expression completely abolished the ability of MBH insulin to suppress HGP (Figure 5, B–D). Peripheral glucose uptake was unaffected by CA-S6K (Figure 5E). Thus, activation of S6K in the MBH was sufficient to induce insulin resistance in the liver. CA-S6K expression also resulted in impaired MBH insulin–stimulated Akt Thr308 and Ser473 phosphorylation (Figure 6), suggesting that the mechanism underlying hypothalamic CA-S6K–induced insulin resistance involves negative feedback on more proximal components of the insulin signaling pathway.

We next investigated whether MBH overexpression of CA-S6K is able to induce hepatic insulin resistance under hyperinsulinemic clamp conditions. The glucose infusion rate tended to be lower in CA-S6K rats (Figure 7A), but did not differ significantly from the controls. HGP in CA-S6K animals was significantly greater than that in LacZ controls (Figure 7, B and C). Analysis of MBH samples following the clamp period demonstrated that CA-S6K animals also had significantly increased serine phosphorylation of IRS-1 (Figure 7E) and S6 ribosomal protein (Figure 7F) relative to LacZ controls, providing further functional validation of the CA-S6K adenovirus.

MBH inhibition of the mTOR/S6K pathway reverses HFD-induced insulin resistance. To examine whether activation of hypothalamic S6K is required for the onset of nutrient-dependent hypothalamic and hepatic insulin resistance during HFD feeding, we used 2 different loss-of-function adenoviruses to selectively decrease the activity of the mTOR/S6K pathway in the MBH of rats fed HFD for 1 d. In cultured cells, glucose and leucine have previously been shown to enhance Ser307 and Ser636/639 phosphorylation of IRS-1, while kinase-dead, dominant-negative S6K (DN-S6K) and

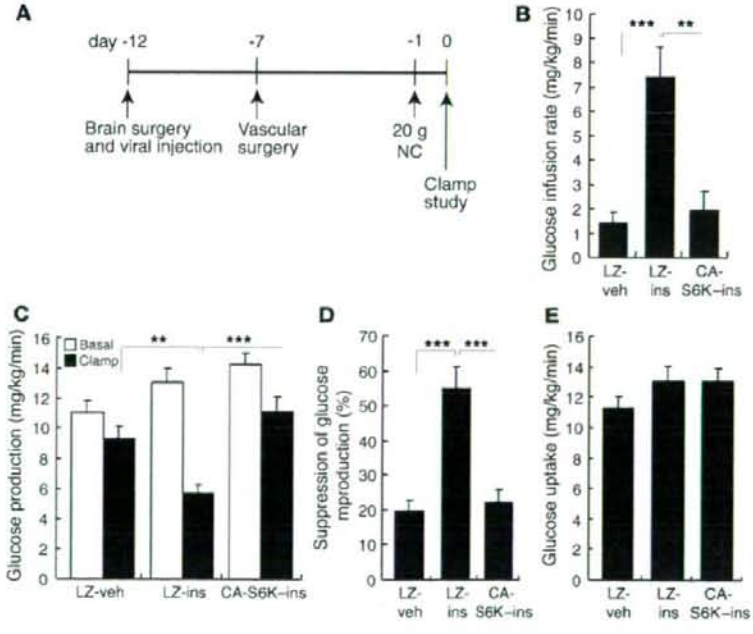

Figure 5
Hypothalamic overexpression of CA-S6K leads to insulin resistance in the basal pancreatic clamp. (**A**) Protocol for surgery, viral injection, and the insulin clamp study. (**B**) Glucose infusion rate required to maintain euglycemia during the clamp period. (**C**) Glucose production during basal and clamp periods. (**D**) Clamp/basal HGP suppression ratio. (**E**) Peripheral glucose uptake during the clamp period. LZ, LacZ. $^{**}P < 0.01$; $^{***}P < 0.001$.

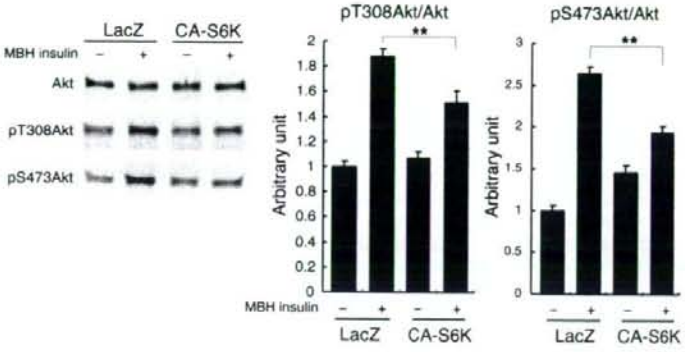

Figure 6
Hypothalamic overexpression of CA-S6K blunts Akt phosphorylation. After 5 h of fasting, 4 μU insulin was infused into the MBH, and 15 min later, the MBH was harvested and analyzed. MBH lysates were blotted with anti–phospho-Thr308 and anti–phospho-Ser473 Akt antibodies. Results are shown as representative bands with quantitation. $^{**}P < 0.01$.

dominant-negative Raptor inhibit phosphorylation at these sites (25, 26). We constructed adenoviruses encoding either a kinase-dead S6K (Figure 8A) that functions in a dominant interfering manner (25, 27–29) or a C terminal–truncated Raptor (Raptor/ΔCT; Figure 8C) that inhibits S6K activity (30) and IRS-1 serine phosphorylation by a mechanism involving uncoupling of the target of rapamycin complex 1 (TORC1; refs. 26, 31). Immunoblotting confirmed MBH expression of DN-S6K and Raptor/ΔCT after virus injection (Figure 8, B and D). These constructs have been functionally validated in prior in vivo studies: transgenic overexpression of the K100Q mutant of S6K in *Drosophila* larvae modifies food preferences (29), and hepatic overexpression of Raptor/ΔCT adenovirus inhibits hepatic S6K activity (32). We also performed functional validations of these viral vectors in GT1-7 hypothalamic cell lines and found that both viruses suppressed insulin-induced serine phosphorylation of IRS-1 at inhibitory sites as well as S6 ribosomal protein (Figure 8E). Our observations extend previous results (26, 31) and indicate that S6K mediates negative feedback regulation of insulin signaling in hypothalamic cell lines. Moreover, in the MBH of 1 d-HFD rats, DN-S6K overexpression suppressed phosphorylation of S6 ribosomal protein (Figure 8F) and Raptor/ΔCT overexpression suppressed S6K activity (Figure 8G), validating the inhibition of TORC1 by these 2 adenoviruses in vivo.

We injected these 2 viruses, as well as LacZ, and 12 d later performed insulin clamp studies after 1 d of feeding with either NC or HFD (Figure 9A). During the clamp study, MBH insulin failed to suppress glucose production in HFD-fed rats expressing LacZ, an observation similar to that in HFD-fed rats without viral treatment (Figure 9, B–D). Overexpression of either DN-S6K or Raptor/ΔCT in the MBH of HFD-fed rats completely reversed the impairment in MBH insulin action. In the presence of basal insulin, the rate of glucose infusion required to maintain euglycemia was marginal in LacZ-injected HFD-fed rats (Figure 9B). However, in HFD-fed rats with MBH DN-S6K or Raptor/ΔCT injection, glucose had to be infused systemically to prevent hypoglycemia (Figure 9B). The increased glucose infusion was caused by suppression of glucose production (Figure 9, C and D), similar to that observed in rats on NC. Glucose uptake was unaffected under all conditions examined (Figure 9E).

Overexpression of either DN-S6K or Raptor/ΔCT in the MBH normalized hypothalamic insulin signaling in 1-d HFD fed rats. DN-S6K or Raptor/ΔCT also enhanced insulin-induced tyrosine phosphorylation of IRS-1 (Figure 10A), Akt Thr308 (Figure 10B), and Akt Ser473 (Figure 10C) phosphorylation. These data suggest that inhibition of endogenous S6K in the MBH of HFD-fed rats reverses diet-induced insulin resistance by blocking negative feedback at the level of IRS-1. Our findings do not, however, rule out the possibility that mTOR itself inhibits insulin signaling via serine phosphorylation of IRS-1, independently of S6K. In this context, some part of the rescue effect achieved using Raptor/ΔCT may be the result of uncoupling of mTOR/Raptor from its substrate IRS-1, rather than inhibition of S6K. However, the effect of DN-S6K was quite similar to that of Raptor/ΔCT, again suggesting that MBH S6K is necessary for the establishment of hepatic insulin resistance with 1-d HFD feeding.

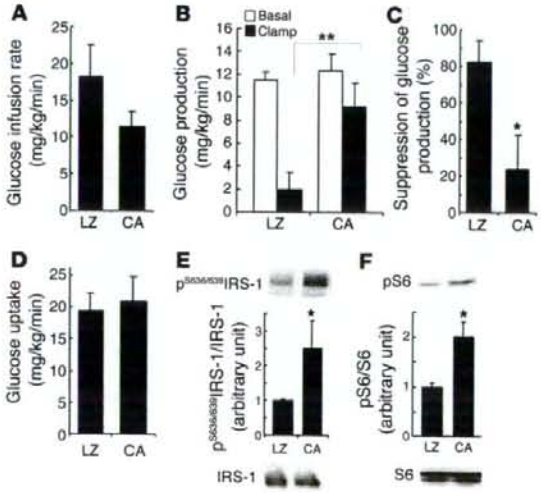

Figure 7
Hypothalamic overexpression of CA-S6K leads to insulin resistance under hyperinsulinemic-euglycemic clamp conditions. (**A**) Glucose infusion rate required to maintain euglycemia during the clamp period. (**B**) Glucose production during basal and clamp periods. (**C**) Clamp/basal HGP suppression ratio. (**D**) Peripheral glucose uptake during the clamp period. (**E**) Phosphoserine IRS-1 and (**F**) phosphoserine S6 at the end of the clamp study. Graphs show the ratio of phosphoproteins to total proteins. $^{*}P < 0.05$ versus LacZ. $^{**}P < 0.01$.